ARTICLES
https://doi.org/10.1038/s41593-018-0288-9
nature neuroscience

GABA and glutamate neurons in the VTA regulate sleep and wakefulness

Xiao Yu[1,8], Wen Li[2,8], Ying Ma[1], Kyoko Tossell[1], Julia J. Harris[1,3], Edward C. Harding[1], Wei Ba[1], Giulia Miracca[1], Dan Wang[2], Long Li[2], Juan Guo[2], Ming Chen[4], Yuqi Li[1], Raquel Yustos[1], Alexei L. Vyssotski[5], Denis Burdakov[3], Qianzi Yang[2], Hailong Dong[2*], Nicholas P. Franks[1,6,7*] and William Wisden[1,6,7*]

We screened for novel circuits in the mouse brain that promote wakefulness. Chemogenetic activation experiments and electroencephalogram recordings pointed to glutamatergic/nitrergic (NOS1) and GABAergic neurons in the ventral tegmental area (VTA). Activating glutamatergic/NOS1 neurons, which were wake- and rapid eye movement (REM) sleep-active, produced wakefulness through projections to the nucleus accumbens and the lateral hypothalamus. Lesioning the glutamate cells impaired the consolidation of wakefulness. By contrast, activation of GABAergic VTA neurons elicited long-lasting non-rapid-eye-movement-like sleep resembling sedation. Lesioning these neurons produced an increase in wakefulness that persisted for at least 4 months. Surprisingly, these VTA GABAergic neurons were wake- and REM sleep-active. We suggest that GABAergic VTA neurons may limit wakefulness by inhibiting the arousal-promoting VTA glutamatergic and/or dopaminergic neurons and through projections to the lateral hypothalamus. Thus, in addition to its contribution to goal- and reward-directed behaviors, the VTA has a role in regulating sleep and wakefulness.

We still do not know all of the circuitry in mammals regulating wakefulness and sleep[1–4]. Broadly, wakefulness is promoted by ascending aminergic and peptidergic systems[1,5–8]. GABAergic and glutamatergic pathways can also induce wakefulness and physical activity[9–17]. On the other hand, sleep is promoted by GABAergic/peptidergic and glutamatergic/nitrergic neurons that inhibit the wake-promoting neurons[3,18–23].

Here, we describe a non-hypothesis-driven chemogenetic search for further circuitry controlling vigilance states, and unexpectedly converge on the VTA. The VTA is intensively investigated for its regulation of goal- and reward-directed and social behaviors[24–28]. As well as dopamine neurons (VTA^{DA}), the VTA contains GABAergic and glutamatergic neurons, which independently project out of the VTA[24,29,30]. These GABA and glutamate neurons are believed to control reward- and goal-directed and social behaviors[31,32]. These behaviors require wakefulness, and indeed VTA^{DA} neurons are selectively wake- and rapid eye movement (REM) sleep-active, and actually promote wakefulness[5,8,33]. Complimenting this work, we find that VTA glutamate/NOS1 and GABA neurons increase and decrease wakefulness, respectively. The VTA is, therefore, a node whose circuitry potently influences vigilance state.

Results

A chemogenetic search for glutamatergic circuitry enhancing wakefulness. We searched for glutamatergic neurons in the posterior hypothalamic–midbrain area (PH/MB) that could promote wakefulness (Fig. 1). By injecting adeno-associated virus (AAV)-DIO-hM3Dq-mCherry into *Vglut2-ires-Cre* mice, we expressed the excitatory hM3Dq DREADD receptor in *Vglut2* neurons in progressively more defined locations (Fig. 1). (Note: for the following series of experiments, clozapine-N-oxide (CNO; 1 mg kg^{-1}) was injected intraperitoneally (i.p.) at the start of 'lights on', when the mice had their maximal sleep drive. Injecting CNO (1 mg kg^{-1}) i.p. into AAV-naïve *Vglut2-ires-Cre* mice—that is, mice not injected with AAV—did not produce any changes in the amounts of sleep or wakefulness (Supplementary Fig. 1a).)

We obtained dramatic results from large-volume injections of AAV-DIO-hM3Dq-mCherry into the PH/MB of *Vglut2-ires-Cre* mice ($(PH/MB)_L^{Vglut2}$-hM3Dq mice) (Fig. 1a). Following CNO injections, 100% wakefulness was induced for 12 h compared with saline-injected control mice (Fig. 1b,c). In these $(PH/MB)_L^{Vglut2}$-hM3Dq mice, hM3Dq-mCherry receptor expression (determined by mCherry staining) was found throughout the lateral hypothalamus (LH), dorsal medial hypothalamus, ventral medial hypothalamus, mammillary area, tuberomammillary area, supramammillary area, VTA, and interpeduncular nucleus (IPN). A smaller AAV injection volume into the PH/MB of *Vglut2-ires-Cre* mice resulted in hM3Dq expression in the LH, mammillary area, and VTA ($(PH/MB)_S^{Vglut2}$-hM3Dq mice, see Fig. 1d). CNO i.p. injection into these $(PH/MB)_S^{Vglut2}$-hM3Dq mice produced continuous wakefulness for approximately 5 h, followed by enhanced wakefulness for another 7 h (Fig. 1e,f). Restricting hM3Dq expression to the LH and activating with systemic CNO also produced extended wakefulness (Fig. 1g–i).

By contrast, restricting hM3Dq expression to glutamatergic neurons in the mammillary area of *Vglut2-ires-Cre* mice (Fig. 1j and Supplementary Fig. 2a, M^{Vglut2}-hM3Dq mice), and giving CNO, did not produce arousal above that resulting from baseline saline injections (Fig. 1k,l). Restricting hM3Dq receptor expression to the

[1]Department of Life Sciences, Imperial College London, London, UK. [2]Department of Anesthesiology & Perioperative Medicine, Xijing Hospital, Xi'an, Shanxi, China. [3]The Francis Crick Institute, London, UK. [4]iHuman Institute, ShanghaiTech University, Shanghai, China. [5]Institute of Neuroinformatics, University of Zürich/ETH Zürich, Zürich, Switzerland. [6]Centre for Neurotechnology, Imperial College London, London, UK. [7]UK Dementia Research Institute, Imperial College London, London, UK. [8]These authors contributed equally: Xiao Yu, Wen Li. *e-mail: hldong6@hotmail.com; n.franks@imperial.ac.uk; w.wisden@imperial.ac.uk

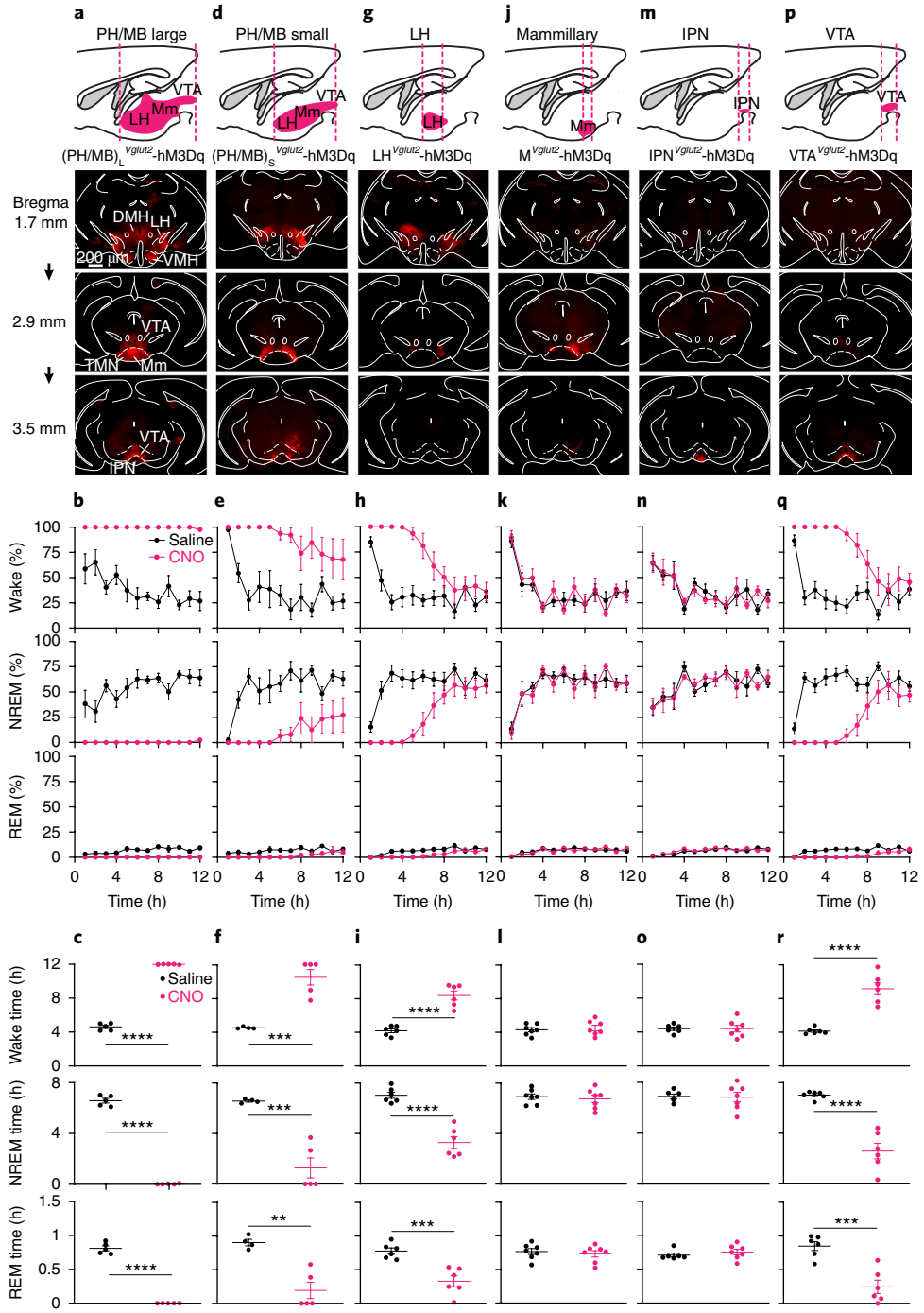

Fig. 1 | Chemogenetic mapping for novel glutamatergic areas in the PH/MB that promote wakefulness identifies the VTA. AAV-DIO-hM3Dq-mCherry was injected into different areas of the brain of Vglut2-ires-Cre mice. AAV expression was determined by immunocytochemistry for mCherry (red). The images show the actual mCherry staining. **a**–**c**, AAV injection into a large volume of PH/MB (PH/MB)$_L$. The experiment in **a** was repeated independently five times. The graphs show percentage of wake, NREM, and REM sleep and how these states vary with saline ($n=5$ mice) or CNO ($n=5$ mice) i.p. injections. **d**–**f**, AAV was injected into a smaller volume of PH/MB (PH/MB)$_s$, and sleep–wake states were scored as above after saline ($n=4$ mice) or CNO ($n=5$ mice) i.p. injections. The experiment in **d** was repeated independently five times. **g**–**i**, AAV injection was restricted to the LH, and sleep–wake states were scored following saline and CNO injection after saline ($n=6$ mice) or CNO ($n=6$ mice) i.p. injections. The experiment in **g** was repeated independently six times. **j**–**l**, AAV injection was restricted to the mammillary area, and sleep–wake states scored following saline ($n=7$ mice) and CNO ($n=7$ mice) i.p. injection. The experiment in **j** was repeated independently five times. See Supplementary Fig. 2a for examples of hM3Dq-mCherry expression in individual mice. **m**–**o**, AAV injection was restricted to the IPN, and sleep–wake states were scored following saline ($n=6$ mice) and CNO ($n=7$ mice) i.p. injection. The experiment in **m** was repeated independently six times. See Supplementary Fig. 2b for examples of individual hM3Dq-mCherry expression. **p**–**r**, AAV injection was restricted to the VTA, and sleep–wake states were scored following saline ($n=6$) and CNO ($n=6$) i.p. injection. The experiment in **p** was repeated independently six times. See Supplementary Fig. 2c for examples of hM3Dq-mCherry expression in individual mice. DMH, dorsomedial hypothalamus; Mm, medial mammillary area; TMN, tuberomammillary area; VMH, ventromedial hypothalamus. All error bars represent the s.e.m. $^{**}P<0.01$, $^{***}P<0.001$, $^{****}P<0.0001$; two-sided unpaired t test. For detailed statistical information, see Supplementary Table 1.

IPN of *Vglut2-ires-Cre* mice (Fig. 1m and Supplementary Fig. 2b, IPN^{Vglut2}-hM3Dq mice), and subsequent injection of CNO, also did not elicit arousal compared with saline injection (Fig. 1n,o).

Glutamatergic neurons in the VTA produce wakefulness. We next limited hM3Dq receptor expression to the VTA of *Vglut2-ires-Cre* mice to make VTA^{Vglut2}-hM3Dq mice (Fig. 1p and Supplementary Fig. 2c). Following 1 mg kg^{-1} CNO i.p. injection, there was 5 h of 100% wakefulness; the extent of wakefulness remained elevated for nearly the entire 'lights on' period (Fig. 1q,r). (Note: as a further control for the specificity of CNO's actions, we injected AAV-DIO-mCherry into the VTA of *Vglut2-ires-Cre* mice; CNO injection (i.p.) into these *VTA^{Vglut2}-mCherry* mice had no effect on the amounts of sleep or wakefulness (Supplementary Fig. 1c).)

Of the brain regions that we injected, the VTA^{Vglut2} population that promotes wakefulness had not to our knowledge previously been identified in this role, and so we decided to study these cells in detail. We first confirmed that these neurons were excited by CNO in VTA^{Vglut2}-hM3Dq mice. One h after CNO i.p. injection into VTA^{Vglut2}-hM3Dq mice, cFos protein was elevated in hM3Dq-expressing VTA^{Vglut2} neurons (saline: 41 ± 4, CNO: 378 ± 36 cFos-positive cells), confirming excitation of VTA^{Vglut2} neurons (Supplementary Fig. 2d). Looking at the CNO-evoked electroencephalogram (EEG) spectra of VTA^{Vglut2}-hM3Dq mice (Supplementary Fig. 2e), the excitation of VTA^{Vglut2} neurons produced higher theta (8 Hz) activity (Supplementary Fig. 2f) but the electromyogram (EMG) signal did not change (Supplementary Fig. 2f). Activation of VTA^{Vglut2} neurons also strongly increased the latency to both non-rapid eye movement (NREM) and REM sleep (Supplementary Fig. 2g). However, excitation of VTA^{Vglut2} neurons did not cause hyperactivity (Supplementary Fig. 2h). In an open field assay, the CNO-injected (i.p.) mice did not move further than saline-injected mice, but stayed awake for an extended period.

Confirming the behavioral effects of the chemogenetic activation of VTA^{Vglut2} neurons, optogenetic activation of VTA^{Vglut2} neurons with ChR2 also increased wakefulness (Supplementary Fig. 3a–c).

VTA^{Vglut2} neurons consolidate wakefulness during the sleep–wake cycle. To investigate how VTA^{Vglut2} neurons influence the sleep–wake cycle over 24 h, we genetically ablated VTA^{Vglut2} neurons using AAV-DIO-CASP3 to produce VTA^{Vglut2}-CASP3 mice (Fig. 2a and Supplementary Fig. 3d). About 80% of the VTA^{Vglut2} neurons were destroyed (Supplementary Fig. 3d). Chronic lesioning of VTA^{Vglut2} cells reduced wakefulness, and increased NREM sleep, but only during the 'lights off' phase (Fig. 2b). Looking at the sleep–wake microarchitecture, wake consolidation was impaired, with more episodes and shorter episode durations of wake (Fig. 2c), and with more transitions between wake and NREM sleep (Fig. 2d), again with the phenotype appearing selectively during 'lights off'.

VTA^{Vglut2} neurons are selectively wake- and REM sleep-active. To determine when during the natural sleep–wake cycle the VTA^{Vglut2} neurons were active, we made VTA^{Vglut2}-GCaMP6 mice (Fig. 2e), then recorded Ca^{2+} signals by fiber photometry (Fig. 2f and Supplementary Fig. 3e). (Note: we used GCaMP6s for all of this and all subsequent photometry experiments.) The Ca^{2+} signal increased selectively during wakefulness and REM sleep (Fig. 2f,g), and with novel objects and female scents (Supplementary Fig. 3e). During NREM sleep, the VTA^{Vglut2} neurons had lower Ca^{2+} signals (Fig. 2f,g). At the transitions between the vigilance states, the ratio of the change in fluorescence intensity relative to the resting baseline fluorescence intensity ($\Delta F/F$ ratio) increased from NREM to wake and from NREM to REM sleep (Fig. 2h), but decreased from wakefulness to NREM. The $\Delta F/F$ ratio changed little during REM sleep to wake transitions (Fig. 2h). (As controls, no changes in the $\Delta F/F$ ratio were found by photometry between vigilance states in VTA^{Vglut2}-GFP mice (Supplementary Fig. 3f,g); furthermore, there was no bleaching of the signal in VTA^{Vglut2}-GCaMP6s mice, as the $\Delta F/F$ ratios stayed constant over 6 h (Supplementary Fig. 3h).)

VTA^{Vglut2} neurons promote wakefulness independently of dopamine. Dopamine neurons in the VTA promote wakefulness[5,8], so we tested whether the wake-promoting effect of VTA^{Vglut2} neurons depended on dopamine. We first verified that VTA^{Vglut2} neurons are largely distinct from VTA dopamine neurons. Immunohistochemistry confirmed that only 26 ± 1.6% of the *Vglut2* cells were tyrosine hydroxylase-positive (Supplementary Fig. 4a,b), as shown previously[24]. Unlike dopamine neurons, VTA^{Vglut2} cells were mostly located in the midline VTA nuclei—the rostral linear nucleus and the interfascicular nucleus (Supplementary Fig. 4b)[24,34]. Thus, the majority of VTA^{Vglut2} and VTA^{DA} neurons are distinct populations. We next chemogenetically activated the VTA^{Vglut2} neurons in VTA^{Vglut2}-hM3Dq mice with CNO in the presence of systemically administered dopamine antagonists SCH-23390 and raclopride for D1 and D2/D3 receptors, respectively (Supplementary Fig. 4c,d) (note: mice were injected i.p. with the dopamine receptor antagonists 30 minutes before CNO i.p. injection—please see Methods for drug concentrations). Even when dopamine receptors were blocked, VTA^{Vglut2} neurons still promoted wakefulness (Supplementary Fig. 4d).

VTA^{Vglut2} neurons promote wakefulness via the nucleus accumbens (NAc) and the LH. To identify the brain areas that participate in generating the VTA^{Vglut2}-mediated wakefulness, we mapped cFos activity in VTA^{Vglut2}-hM3Dq mice. Following CNO i.p. injection, increased numbers of cFos-positive cells were identified in multiple

Fig. 2 | VTA^{Vglut2} neurons consolidate wakefulness and are selectively wake- and REM sleep-active. a, Lesioning of VTA^{Vglut2} neurons. Injection of AAV-DIO-GFP (control) or AAV-DIO-GFP and AAV-DIO-taCASP3-TEV into the VTA area of *Vglut2-ires-Cre* mice. Pictures show GFP control expression in the VTA area of VTA^{Vglut2}-GFP mice and that this GFP expression has been greatly diminished in the VTA^{Vglut2}-CASP3 mice. The experiment was repeated independently six times. IF, interfascicular nucleus; PN, paranigral nucleus; RLi, rostral linear nucleus. **b**, Lesioning of VTA^{Vglut2} neurons. Percentages of wake, NREM, and REM sleep in control VTA^{Vglut2}-GFP mice ($n = 7$ mice) and VTA^{Vglut2}-CASP3 mice ($n = 8$ mice), and the total vigilance times in the 'lights on' and 'lights off' periods. **c**,**d**, Lesioning of VTA^{Vglut2} neurons. Episode number and duration for wake, NREM, and REM sleep, and vigilance state transitions during the 'lights off' periods in VTA^{Vglut2}-GFP control mice ($n = 7$ mice) and VTA^{Vglut2}-CASP3 mice ($n = 8$ mice). **e**, Fiber photometry for VTA^{Vglut2} neurons. Injection of AAV-DIO-GCaMP6 into the VTA of the *Vglut2-ires-Cre* mice. The experiment was repeated independently seven times. GCaMP6 expression can be detected in the VTA area and the trace of where the optical fiber was placed is marked. **f**, Fiber photometry Ca^{2+} spectra (bottom trace) recorded in the VTA of VTA^{Vglut2}-GCaMP6 mice aligned with the EEG (middle trace) and EMG (top trace) spectra during wakefulness, NREM, and REM sleep. 'Epoch' indicates vigilance state: blue, wake; green, NREM sleep; magenta, REM sleep. **g**, Fiber photometry $\Delta F/F$ ratio of the Ca^{2+} signal in *VTA^{Vglut2}-GCaMP6* mice during wakefulness, NREM sleep, and REM sleep ($n = 7$ mice; 38 sessions). **h**, Detail of how the Ca^{2+} photometry signal in *Vglut2* neurons of VTA^{Vglut2}-GCaMP6 mice changes at the boundaries of the vigilance states ($n = 7$ mice). Ca^{2+} photometry $\Delta F/F$ ratio (bottom trace) in the VTA^{Vglut2}-GCaMP6 mice aligned with the extracted δ power in the EEG, the EEG spectrum itself, and EMG during wakefulness, NREM, and REM sleep. 'Epoch' indicates vigilance state as in **f**. Gray-shaded regions represent s.e.m. $^{*}P < 0.05$, $^{**}P < 0.01$, $^{****}P < 0.0001$; for **b**–**d**, two-sided unpaired *t* test; for **g**, one-way analysis of variance (ANOVA). All error bars represent s.e.m. For detailed statistical information, see Supplementary Table 1.

brain regions (Fig. 3a and Supplementary Fig. 5a,b). cFos expression was particularly activated in the LH, NAc, and ventral pallidum (Fig. 3a and Supplementary Fig. 5a,b). In the LH, 60% of cFos-expressing cells that were activated by CNO i.p. injections were also orexin-positive compared with the low number of cFos-expressing cells following saline injection (Supplementary Fig. 5c).

We then undertook ChR2-based circuit mapping of the VTA^{Vglut2} neurons in VTA^{Vglut2}-ChR2-EYFP mice (Fig. 3b and Supplementary Fig. 5d). Consistent with the cFos activation data, there was a dense projection of VTA^{Vglut2} neurons to the LH and NAc (Fig. 3b and Supplementary Fig. 5c), as described previously[29,30,35,36]. To test whether the VTA^{Vglut2}→LH or VTA^{Vglut2}→NAc projections

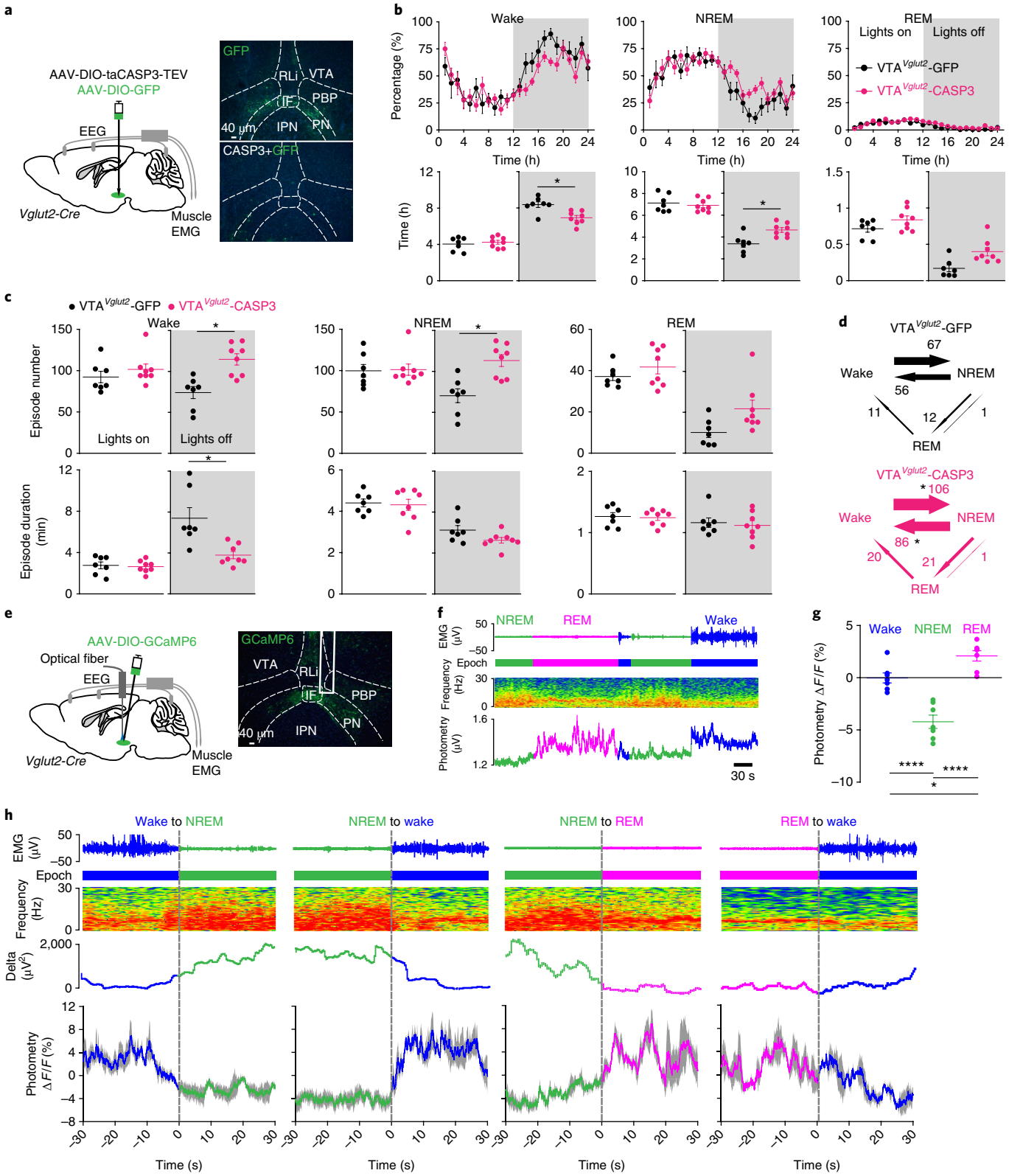

can promote wakefulness, we placed optical fibers into the LH and NAc of VTA^{Vglut2}-ChR2-EYFP mice to stimulate the terminals (Fig. 3c–f). Optically stimulating VTA^{Vglut2} fibers in the LH strongly and consistently promoted waking from NREM sleep (Fig. 3c and Supplementary Fig. 6a); chronic optical stimulation for 3 h maintained wakefulness (Fig. 3d). Similarly, optogenetic stimulation of the VTA^{Vglut2} terminals in the NAc promoted waking from NREM sleep (Fig. 3e and Supplementary Fig. 6b) and chronic optogenetic stimulation for 3 h increased wakefulness and reduced NREM and REM sleep (Fig. 3f). Thus, the LH and NAc are two areas contributing to wakefulness when excited by VTA^{Vglut2} neurons.

Nitric oxide synthase marks wake-promoting VTA^{Vglut2} neurons. To confirm the wake-promoting actions of the VTA^{Vglut2}→LH and VTA^{Vglut2}→NAc projections, we used retrograde-labeling by injecting AAV-Retro-DIO-Chronos-GFP into the LH and NAc of *Vglut2-ires-Cre* mice. We identified many green fluorescent protein (GFP)-positive soma in the VTA (Supplementary Fig. 7a,b). We optogenetically activated the Chronos-GFP retro-labeled cells by inserting optical fibers into the VTA (Supplementary Fig. 7b). Tonic opto-activation increased cFos in these retro-labelled neurons (control: 31 ± 5, stimulation: 206 ± 41) (Supplementary Fig. 7c). Activation of the retro-labeled NAc→VTA^{Vglut2} neurons increased wakefulness (Supplementary Fig. 7d). To profile these retro-labeled VTA^{Vglut2} neurons, we stained VTA^{Vglut2} neurons with a panel of antibodies recognizing neurochemical markers (nitric oxide synthase (NOS1), tyrosine hydroxylase, glutamic acid decarboxylase (GAD67), parvalbumin, somatostatin) (Fig. 4a and Supplementary Fig. 7e). Of these markers, double-labeling of retro-labeled NAc→VTA^{Vglut2} and LH→VTA^{Vglut2} neurons identified that about 68 ± 9% of the GFP-positive cells were immuno-positive for NOS1 (Fig. 4a and Supplementary Fig. 7f), mostly in the midline VTA. This was confirmed by direct double-labeling with VTA^{Vglut2}-ChR2-EYFP neurons and VTA^{Nos1} neurons (Supplementary Fig. 8a,b). About 75 ± 3% of VTA^{Nos1} cells were VTA^{Vglut2}-positive (Supplementary Fig. 8b), as also seen independently[34].

To test whether the VTA^{Nos1} neurons are functionally the same as the VTA^{Vglut2} neurons in producing wakefulness, we chemogenetically activated the VTA^{Nos1} neurons by delivering AAV-DIO-hM3Dq-mCherry into the VTA of *Nos1-ires-Cre* mice (Fig. 4b,c). As for the *VTA^{Vglut2}-hM3Dq* mice, giving 1 mg kg^{-1} CNO i.p. to the VTA^{Nos1}-hM3Dq mice produced sustained wakefulness (100%) for 4 h (Fig. 4c and Supplementary Fig. 8c). Also similar to the VTA^{Vglut2}-hM3Dq mice, the wakefulness produced by i.p.-administered CNO activation of VTA^{Nos1} neurons was not blocked by systemic i.p.-administered dopamine D1 and D2/D3 receptor antagonists (Supplementary Fig. 8d) (note: mice were injected i.p. with the dopamine receptor antagonists 30 minutes before CNO i.p. injection—see Methods for drug concentrations). Thus, the wake-promoting VTA^{Nos1} neurons are a subset of VTA^{Vglut2} neurons. Chemogenetic inhibition of these VTA$^{Vglut2/Nos1}$ neurons, by delivering AAV-DIO-hM4D$_i$-mCherry into the VTA of *Nos1-ires-Cre* mice and giving CNO i.p., decreased wakefulness and produced more NREM sleep (Fig. 4b,d and Supplementary Fig. 8e). Therefore, VTA$^{Vglut2/Nos1}$ neurons can bidirectionally regulate wakefulness. We next mapped projections of VTA^{Nos1} neurons by injecting AAV-DIO-ChR2-EYFP into the VTA of *Nos1-ires-Cre* mice. Similar to VTA^{Vglut2} neurons, VTA^{Nos1} neurons project to the NAc, ventral pallidum, and LH (Supplementary Fig. 8f), again implying that the NOS1-expressing neurons are a subset of the glutamatergic ones.

VTA^{Vgat} neurons limit wakefulness and induce NREM sleep. We next looked for neurons in the VTA that could potentially restrain the wake-promoting activity of the VTA$^{Vglut2/Nos1}$ neurons. The VTA contains many GABAergic neurons (Supplementary Fig. 9a,b)[24,30]. These can be detected by expression of the vesicular GABA transporter (VGAT). We first confirmed that *Vgat* gene-expressing neurons were mostly distinct from dopamine or glutamate neurons: only 0.3 ± 0.1% of these GABAergic neurons (as defined by VTA^{Vgat}-ChR2-EYFP staining) stained with tyrosine hydroxylase (Supplementary Fig. 9a), and 12 ± 0.6% of these VTA^{Vgat} neurons were NOS1-positive; however, these cells were not in the midline but mostly in the lateral part of the VTA (parabrachial pigmented nucleus, PBP), which is distinct from VTA$^{Nos1/Vglut2}$ populations in the midline (Supplementary Fig. 9b)[34].

To examine whether VTA^{Vgat} neurons contribute to sleep–wake regulation, AAV-DIO-hM3Dq-mCherry or AAV-DIO-hM4D$_i$-mCherry was injected into the VTA of *Vgat-ires-Cre* mice to generate VTA^{Vgat}-hM3Dq and VTA^{Vgat}-hM4D$_i$ mice, respectively (Fig. 5a and Supplementary Fig. 9c,d). CNO injection i.p. into VTA^{Vgat}-hM3Dq mice produced sustained (80%) NREM sleep for 6 h (Fig. 5b), with continuous δ power in the EEG. Following CNO administration i.p., the latency to NREM sleep was reduced to about 10 minutes compared with saline administration (Fig. 5c). However, latency to REM sleep was notably increased—there was no REM sleep in the first 6 h (Fig. 5c). (Note: we did several further controls for the specificity of CNO's actions to ensure it was not acting as a sedative after conversion to clozapine[37]. We injected 1 mg kg^{-1} CNO i.p. into both AAV-naïve *Vgat-ires-Cre* mice—that is, mice that had not received any AAV injections (Supplementary Fig. 1b)—and into VTA^{Vgat}-mCherry mice (produced by injecting AAV-DIO-mCherry into the VTA of *Vgat-ires-Cre* mice). In neither of these types of mice did CNO alter the amounts of sleep or wakefulness compared with saline-injected controls (Supplementary Fig. 1d). In a separate study[21], we similarly found that CNO systemically injected i.p. at the higher concentration of 5 mg kg^{-1} into AAV-naïve *Vgat-ires-Cre*

Fig. 3 | VTA^{Vglut2} neurons promote wakefulness by their projections to the LH and NAc. a, cFos-based activity mapping of brain regions after exciting VTA^{Vglut2} neurons. In VTA^{Vglut2}-hM3Dq mice, labeled axons mainly project from the VTA to the LH and NAc. cFos protein expression in neurons of the LH and NAc of VTA^{Vglut2}-hM3Dq mice 2 h after saline or CNO i.p. injection at zeitgeber time (ZT) 0. The red in the histology figure is the primary fluorescence of the hM3Dq-mCherry-positive axons coming from the VTA area; the cFos immunohistochemistry is shown in green. The experiment was repeated independently six times. CPu, caudate-putamen; MS, medial septum; PeF, perifornical area; 3V, third ventricle; VP, ventral pallidum. **b**, Axonal projections of VTA^{Vglut2} neurons. AAV-DIO-ChR2-EYFP was delivered into the VTA of *Vglut2-ires-Cre* mice, and axons projecting to the LH and NAc were strongly labeled. The experiment was repeated independently four times. TH, tyrosine hydroxylase. **c**,**d**, To functionally investigate the VTA^{Vglut2}→LH projection, an optical fiber was placed into the LH area of VTA^{Vglut2}-ChR2-EYFP mice. **c**, Mice were given 120 s of optostimulation (20 Hz) during NREM sleep ('lights on' period) and the percentages and times for wake and NREM were scored (control: $n = 6$ mice, 23 trials; ChR2: $n = 6$ mice, 21 trials). **d**, *VTA^{Vglut2}-ChR2-EYFP* mice (control: $n = 8$ mice; ChR2: $n = 8$ mice) were given 3 h of optostimulation at the start of the sleep period ('lights on' period) and the percentages and times for wake, NREM, and REM sleep were scored. **e**,**f**, To functionally investigate the VTA^{Vglut2}→NAc projection, an optical fiber was placed into the NAc area of VTA^{Vglut2}-ChR2-EYFP mice. **e**, Mice were given 120 s of optostimulation (20 Hz) during NREM sleep ('lights on' period) and the percentages and times for wake and NREM were scored (control: $n = 9$ mice, 21 trials; ChR2: $n = 10$ mice, 20 trials). **f**, VTA^{Vglut2}-ChR2-EYFP mice (control: $n = 6$ mice; ChR2: $n = 6$ mice) were given 3 h of optostimulation at the start of sleep ('lights on' period) and the percentages and times for wake, NREM, and REM sleep were scored. $^{**}P < 0.01$, $^{***}P < 0.001$, $^{****}P < 0.0001$; for **c** and **e**, two-sided Mann–Whitney *U* test; for **d** and **f**, two-sided unpaired *t* test. All error bars represent the s.e.m. For **c** and **e**, the shaded region represents s.e.m. For detailed statistical information, see Supplementary Table 1.

mice also did not induce NREM sleep above the background of sleep occurring following saline injection[21].)

In converse experiments with chemogenetic inhibition of VTA^{Vgat} neurons, injecting CNO i.p. into VTA^{Vgat}-hM4D$_i$ mice produced 100% wakefulness for 6 h with sustained theta frequencies in the EEG (Fig. 5d). There was an increased latency to the first NREM and REM sleep bouts to >6 h post-injection of CNO i.p. compared with saline i.p.-injected mice (Fig. 5e).

We next examined whether subtypes of GABAergic neurons can induce NREM sleep. Subtypes of GABAergic neurons in the VTA include those expressing parvalbumin (*Pv*), somatostatin (*Som*), and, in the PBP region, *Nos1*/*Vgat*[34] (see also Supplementary Fig. 9b). We chemogenetically activated VTA^{Pv}, VTA^{Som}, and VTA-PBP$^{Nos1/Vgat}$ populations in the VTA (Supplementary Fig. 10) by expressing hM3Dq-mCherry in these cells. Activation of VTA^{Pv} and VTA^{Som} neurons each produced 3 h of NREM sleep (Supplementary

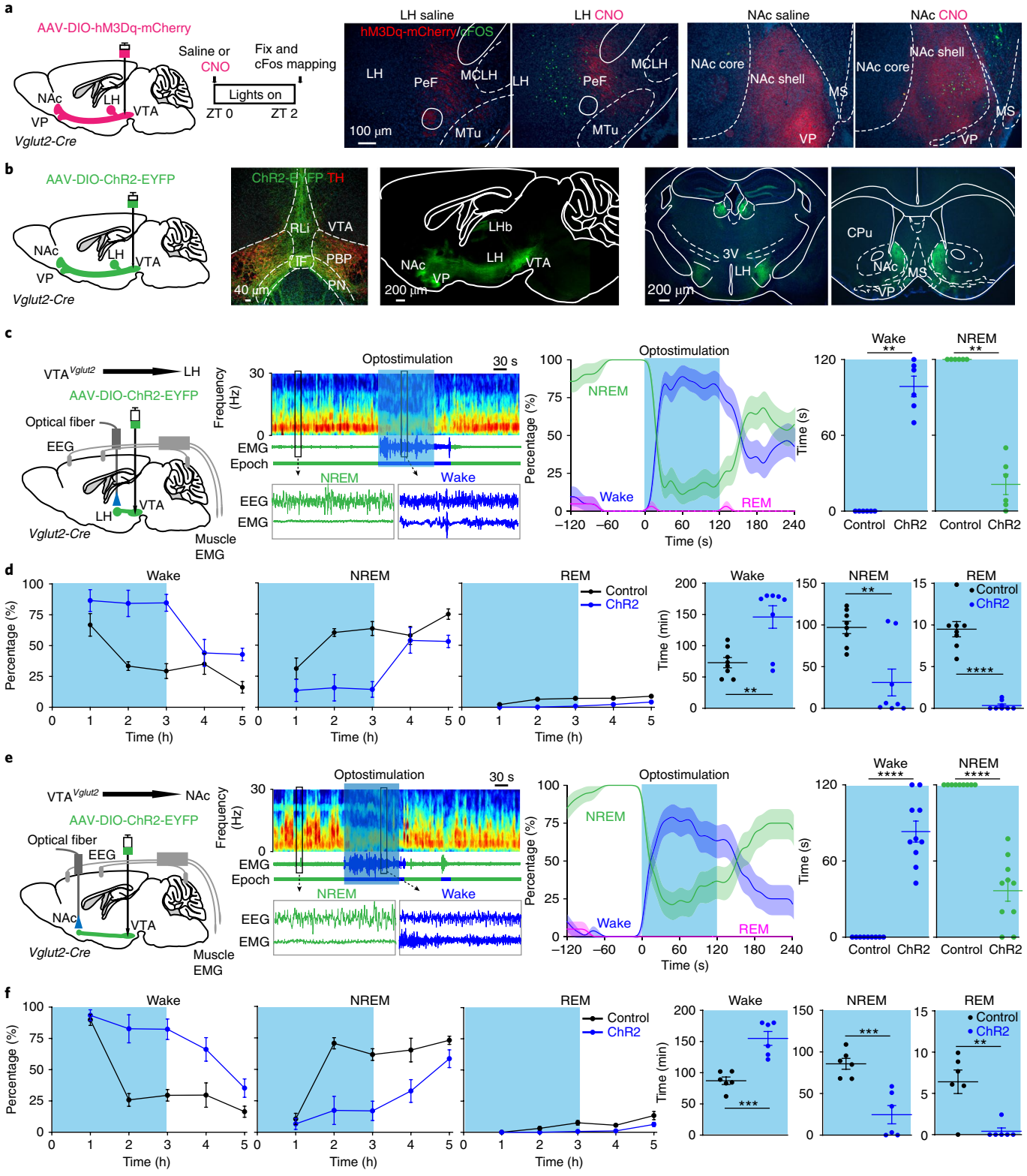

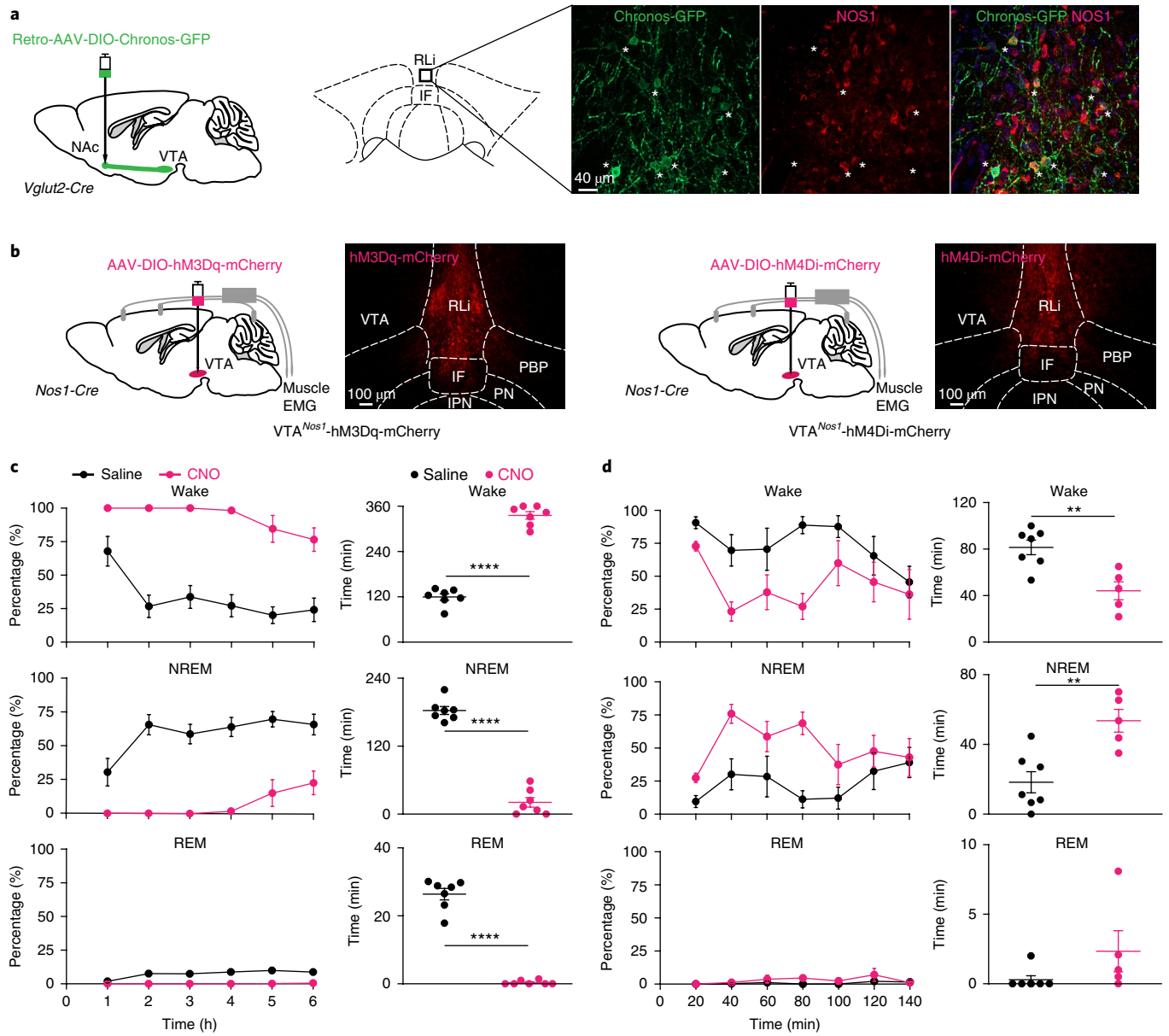

Fig. 4 | VTA^{Vglut2} and VTA^{Nos1} neurons promote wakefulness. a, Retromapping of VTA^{Vglut2}→NAc connections. Retro-AAV-DIO-Chronos-GFP was injected into the NAc of *Vglut2-ires-Cre* mice. Chronos-GFP expression was detected in cells of the VTA, and Chronos-GFP retrolabeled VTA midline soma (from the NAc injection) were double-labeled by immunocytochemistry with NOS1 antisera. The experiment was repeated independently three times. **b**, Testing how VTA^{Nos1} neurons influence vigilance state. AAV-DIO-hM3Dq-mCherry or AAV-DIO-hM4D$_i$-mCherry was injected into the VTA area of *Nos1-ires-Cre* mice. Images show the expression of hM3Dq-mCherry or hM4D$_i$-mCherry in the VTA. The experiment was repeated independently six times. **c**, Excitation of VTA^{Nos1} neurons induces wakefulness. Percentages and times for wake, NREM, and REM sleep after saline ($n=7$ mice) or CNO ($n=7$ mice) i.p. injection at the start of the sleep period ('lights on' period) into VTA^{Nos1}-hM3Dq mice. **d**, Inhibition of VTA^{Nos1} neurons induces NREM sleep. Percentages and times for wake, NREM, and REM sleep after saline ($n=7$ mice) or CNO ($n=5$ mice) i.p. injection during the wake period ('lights off' period) into VTA^{Nos1}-hM4D$_i$ mice. $^{**}P<0.01$, $^{****}P<0.0001$; two-sided unpaired *t* test. All error bars represent s.e.m. For detailed statistical information, see Supplementary Table 1.

Fig. 10). However, activating VTA-PBP$^{Nos1/Vgat}$ neurons did not induce either sleep or wakefulness (Supplementary Fig. 10). Thus, several GABAergic subtypes in the VTA can contribute to induction of NREM sleep, although each group activated individually does not give the full effect obtained with activating VTA^{Vgat} neurons.

Lesioning of VTA^{Vgat} neurons produces continuous wakefulness. To look at VTA^{Vgat} function in the sleep–wake cycle over 24 h, we chronically lesioned VTA^{Vgat} neurons with AAV-DIO-CASP3 (Fig. 6a and Supplementary Fig. 11a). About 88% of the VTA^{Vgat} neurons were destroyed (Supplementary Fig. 11a). In these VTA^{Vgat}-CASP3 mice, there was an increase in wakefulness in both the 'lights on' and 'lights off' periods, but especially during the 'lights off' period—the VTA^{Vgat}-CASP3 animals slept for only 40 minutes, whereas non-lesioned VTA^{Vgat}-GFP control mice slept 4 h in the 12 h of the 'lights off' period (Fig. 6b). During 'lights on', the least active period of the mice, the control mice slept for about 7 h, and the VTA^{Vgat}-CASP3 mice slept for about 6 h (Fig. 6b). During 'lights off', the average NREM episode duration of VTA^{Vgat}-CASP3 mice was much shorter, and transitions between vigilance states were dramatically decreased (Fig. 6c,d). The reduced sleep phenotype of *VTA^{Vgat}-CASP3* persisted unchanged for at least 4 months,

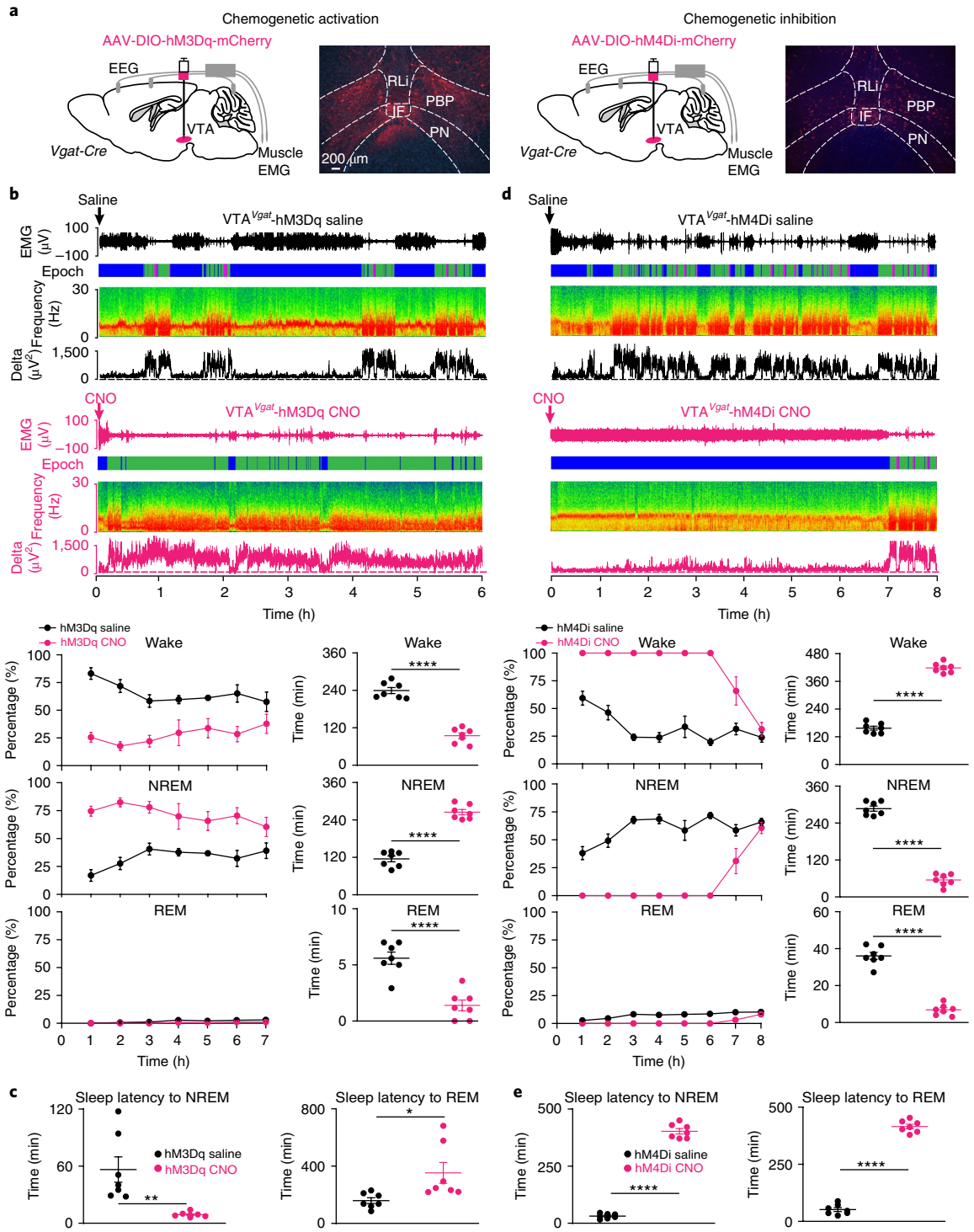

Fig. 5 | Excitation of GABAergic neurons in the VTA induces sleep and their inhibition produces continuous wakefulness. a, Excitation and inhibition of VTA^{Vgat} neurons. AAV-DIO-hM3Dq-mCherry or AAV-DIO-hM4D$_i$-mCherry was injected into the VTA of *Vgat-ires-Cre* mice. Images show the expression of hM3Dq-mCherry or hM4D$_i$-mCherry in the VTA. The experiment was repeated independently six times. **b**, Excitation of VTA^{Vgat} neurons induces NREM sleep and suppresses REM sleep. Two individual EEG and EMG spectra and extracted delta power from the EEG are shown for VTA^{Vgat}-hM3Dq mice that received saline ($n=7$ mice) or CNO ($n=7$ mice) i.p. injection during the wake period ('lights off' period). The percentages and times for wake, NREM, and REM sleep after saline ($n=7$ mice) or CNO ($n=7$ mice) injection are shown. 'Epoch' indicates vigilance state: blue, wake; green, NREM sleep; magenta, REM sleep. **c**, Excitation of VTA^{Vgat} neurons reduces latency to NREM sleep. Latencies to NREM and REM sleep after saline ($n=7$ mice) or CNO ($n=7$ mice) i.p. injection into VTA^{Vgat}-hM3Dq mice. **d**, Inhibition of VTA^{Vgat} neurons induces wakefulness. Two individual EEG and EMG spectra and extracted delta power from the EEG are shown for VTA^{Vgat}-hM4D$_i$ mice that received saline ($n=7$ mice) or CNO ($n=7$ mice) i.p. injection at the start of the sleep period ('lights on' period). The percentages and times for wake, NREM, and REM sleep after saline ($n=7$ mice) or CNO ($n=7$ mice) i.p. injection are shown. 'Epoch' indicates vigilance state, as in **b**. **e**, Inhibition of VTA^{Vgat} neurons increases latency to sleep. Latencies to NREM ($n=7$ mice) and REM sleep ($n=7$ mice) after CNO or saline i.p. injection into VTA^{Vgat}-hM4D$_i$ mice. $^*P<0.05$, $^{**}P<0.01$, $^{****}P<0.0001$; two-sided unpaired *t* test. All error bars represent s.e.m. For detailed statistical information, see Supplementary Table 1.

resulting in the mice having a permanent and substantial sleep deficit (Supplementary Fig. 11b).

VTA^{Vgat} neurons are selectively wake- and REM-active. Based on the chemogenetic and lesioning results, we might have expected VTA^{Vgat} neurons to be NREM sleep-active. To test this, we made VTA^{Vgat}-GCaMP6 mice and measured the activity of VTA^{Vgat} neurons by fiber photometry during different vigilance states of freely moving mice (Fig. 6e). Surprisingly, as for the *Vglut2* neurons, we found that the Ca^{2+} signal for the VTA^{Vgat} neurons actually increased selectively during wakefulness and REM sleep (Fig. 6f). During NREM sleep the VTA^{Vgat} cells had a lower Ca^{2+} signal (Fig. 6f,g). At the transitions between the vigilance states (Fig. 6h), the $\Delta F/F$ ratio decreased from wakefulness to NREM sleep, and increased from NREM sleep to wake, and from NREM to REM sleep (Fig. 6h). Within an individual bout of wake or REM sleep, the Ca^{2+} signal of the VTA^{Vgat} cells did not differ between the earlier and later parts of the bouts (Supplementary Fig. 11c).

To search for NREM sleep-active VTA^{Vgat} neurons that might have been missed by fiber photometry, we used micro-endoscopic calcium imaging of these neurons in VTA^{Vgat}-GCaMP6f mice (Supplementary Fig. 12). We placed a gradient refractive index (GRIN) lens above the VTA, and recorded fluorescence of VTA^{Vgat} neurons during NREM sleep or wakefulness of freely moving mice (Supplementary Fig. 12a). For the single cells that were tracked (16 cells from 4 mice), Ca^{2+} levels in VTA^{Vgat} neurons increased during wake and decreased during NREM sleep (Supplementary Fig. 12b–f). This result further confirmed that VTA^{Vgat} neurons are selectively wake-active.

VTA^{Vgat} neurons reduce wakefulness and induce NREM sleep by both local inhibition and via projections to the LH. Because VTA^{Vgat} neurons are selectively wake- and REM-on, we hypothesized that they are not physiologically triggering NREM sleep, but they are instead limiting wakefulness. To explore how VTA^{Vgat} neurons do this, we conducted ChR2-based mapping of the projections of VTA^{Vgat} axons by delivering AAV-DIO-ChR2-EYFP into the VTA area of *Vgat-ires-Cre* mice. As published previously[38], dense VTA^{Vgat} ChR-positive fibers were found locally in the VTA (Fig. 7a) but also in the LH area (Fig. 7a) and, to some extent, in the lateral habenula (LHb) and dentate granule cells of the hippocampus (Supplementary Fig. 13a); a few fibers were also in the prefrontal cortex (PFC) and lateral preoptic area (Supplementary Fig. 13a). The especially dense VTA^{Vgat} fibers in the VTA indicate strong local inhibition. To test these connections, we did cFos activity mapping by inhibiting VTA^{Vgat} neurons with 1 mg kg^{-1} CNO injected i.p. into VTA^{Vgat}-hM4D$_i$ mice to examine which areas of the brain expressed cFos protein (by disinhibition). After CNO injection i.p., which promoted wakefulness (Fig. 5d), cFos was induced strongly in the VTA and LH (Fig. 7b and Supplementary Fig. 13b,c). Thus, based on cFos expression as a readout of neuronal excitation, VTA^{Vgat} neurons cause inhibition by projecting to the LH, as well as local inhibition in the VTA.

We confirmed directly that VTA^{Vgat} neurons can mediate local inhibition. We prepared acute brain slices containing the midline VTA from *VTA^{Vgat}-ChR2-EYFP* mice, optogenetically activated the VTA^{Vgat} neurons (Fig. 7c), and observed the postsynaptic responses in non-*Vgat* cells. Whole-cell patch clamping confirmed that 87.5% of postsynaptic cells (14 of 16 cells) received either optogenetically evoked inhibitory postsynaptic currents (oIPSCs) only, or both oIPSCs and optogentically evoked excitatory postsynaptic currents (oEPSCs) ((Fig. 7c); 12.5% of cells (2 of 16 cells) had oEPSCs only (Fig. 7c). From the relative peak oIPSC and oEPSC ratios, most non-VGAT cells had significantly larger oIPSCs than oEPSCs (Fig. 7c). From single-cell PCR profiling, these non-*Vgat* neurons with oIPSCs were a mixture of VTA^{Vglut2}, VTA^{DA}, and VTA$^{Vglut2/DA}$ neurons (Fig. 7d); the two cells that responded with only oEPSCs were VTA^{Vglut2} and VTA^{DA} cells. Thus, the majority of non-*Vgat* cells in the midline VTA have a large density of inhibitory input from local VTA^{Vgat} neurons.

Because midline VTA^{Vgat} neurons inhibit midline dopamine neurons, we examined the effect of this local inhibition on wakefulness. We gave D1 and D2/3 receptor antagonists to CNO-injected VTA^{Vgat}-hM4D$_i$ mice (mice were injected i.p. with the dopamine receptor antagonists 30 minutes before CNO i.p. injection—see Methods for drug concentrations). Without dopamine antagonists, CNO inhibition of VTA^{Vgat} neurons caused 6 h of sustained wakefulness (as shown previously in Fig. 5d). With dopamine receptor antagonists, CNO-induced wakefulness was blocked by 20% (Fig. 7e), implying that the sustained wakefulness originating from the inhibited VTA^{Vgat} neurons could be partially due to the activation (disinhibition) of VTA dopamine neurons.

To test whether VTA^{Vgat} neurons use local inhibition to restrict wakefulness, we infused the $GABA_A$ receptor antagonist gabazine (SR95531) into the VTA of CNO i.p.-injected VTA^{Vgat}-hM3Dq mice (please see Methods for gabazine concentration) (Fig. 7f). In the CNO-injected VTA^{Vgat}-hM3Dq mice, gabazine reduced CNO-induced NREM sleep by 40% (Fig. 7f). Thus, the sustained NREM sleep originating from the activated VTA^{Vgat} neurons was partially due to local inhibition of VTA^{Vglut2}, VTA^{DA}, and VTA$^{Vglut2/DA}$ neurons.

As blocking local GABA transmission with gabazine did not completely abolish the ability of activated VTA^{Vgat} neurons to induce sustained NREM sleep, the projections of these VTA^{Vgat} neurons might also contribute. We found that, following CNO inhibition of VTA^{Vgat} neurons in VTA^{Vgat}-hM4Di mice, the number of cFos-expressing cells in the LH was strongly elevated compared with saline injections

Fig. 6 | VTA^{Vgat} neurons inhibit wakefulness; lesioning of VTA*Vgat* neurons produces extended wakefulness, but VTA*Vgat* neurons are selectively wake- and REM-active. a, Lesioning of VTA^{Vgat} neurons. Injection of AAV-DIO-GFP (control) or AAV-DIO-taCASP3-TEV into the VTA area of *Vgat-ires-Cre* mice. Pictures show GFP control expression in the VTA area of VTA^{Vgat}-GFP mice and that this GFP expression has been greatly diminished in the caspase-treated mice. The experiment was repeated independently five times. **b**, Lesioning of VTA^{Vgat} neurons increases wakefulness. Percentages of wake, NREM, and REM sleep in control VTA^{Vgat}-GFP mice ($n=7$ mice) and VTA^{Vgat}-CASP3 mice ($n=5$ mice), and the total vigilance times in the 'lights on' and 'lights off' periods. **c**,**d**, Lesioning of VTA^{Vgat} neurons reduces the transitions between vigilance states and stabilizes wakefulness. Episode number and duration for wake, NREM, and REM sleep, and vigilance state transitions during the 'lights off' periods in VTA^{Vgat}-GFP control mice ($n=7$ mice) and VTA^{Vgat}-CASP3 mice ($n=5$ mice). **e**, Fiber photometry for Ca^{2+} levels in VTA^{Vgat} neurons. Injection of AAV-DIO-GCaMP6 into the VTA of *Vgat-ires-Cre* mice. GCaMP6 expression can be detected in the VTA area and was costained with GABA. The trace of where the optical fiber was placed is illustrated. The experiment was repeated independently seven times. **f**, Fiber photometry for VTA^{Vgat} neurons. Neurons are more active in wake and REM sleep. Ca^{2+} photometry spectra (bottom trace) recorded in the VTA of VTA^{Vgat}-GCaMP6 mice aligned with the EEG (middle trace) and EMG (top trace) spectra during wakefulness, NREM, and REM sleep. 'Epoch' indicates vigilance state: blue, wake; green, NREM sleep; magenta, REM sleep. **g**, Fiber photometry for VTA^{Vgat} neurons. $\Delta F/F$ ratio of the Ca^{2+} photometry signal in *VTA^{Vgat}-GCaMP6f* mice during wakefulness, NREM sleep, and REM sleep ($n=7$ mice, 41 trials). **h**, Fiber photometry for VTA^{Vgat} neurons. Detail of how the Ca^{2+} signal in *Vgat* neurons of VTA^{Vgat}-GCaMP6 mice changes at the boundaries of the vigilance states ($n=7$ mice). 'Epoch' indicates vigilance state as in **f**. Gray-shaded regions represent s.e.m. *P <0.05, **P <0.01, ****P <0.0001; for **b**–**d**, two-sided unpaired t test; for **g**, one-way ANOVA. All error bars represent s.e.m. For detailed statistical information, see Supplementary Table 1.

(Fig. 7b). About 50% of those Fos-positive LH cells were orexin neurons (Supplementary Fig. 13d). By injecting Retro-AAV-DIO-Chronos-GFP into the LH area of *Vgat-ires-Cre* mice, we also detected dense retro-labeled soma in the VTA (Supplementary Fig. 13e).

The results imply that the VTA^{Vgat}→LH projection participates in NREM sleep induction. We therefore placed optical fibers into the LH of VTA^{Vgat}-ChR2-EYFP mice to stimulate the terminals of VTA^{Vgat} neurons (Fig. 8a). Opto-activating VTA^{Vgat} fibers in the LH strongly and consistently initiated wake to NREM sleep transitions (Fig. 8a); Chronic opto-stimulation for 3 h increased NREM sleep and reduced wakefulness and REM sleep (Fig. 8b). Moreover, activation could also maintain NREM sleep, with much longer

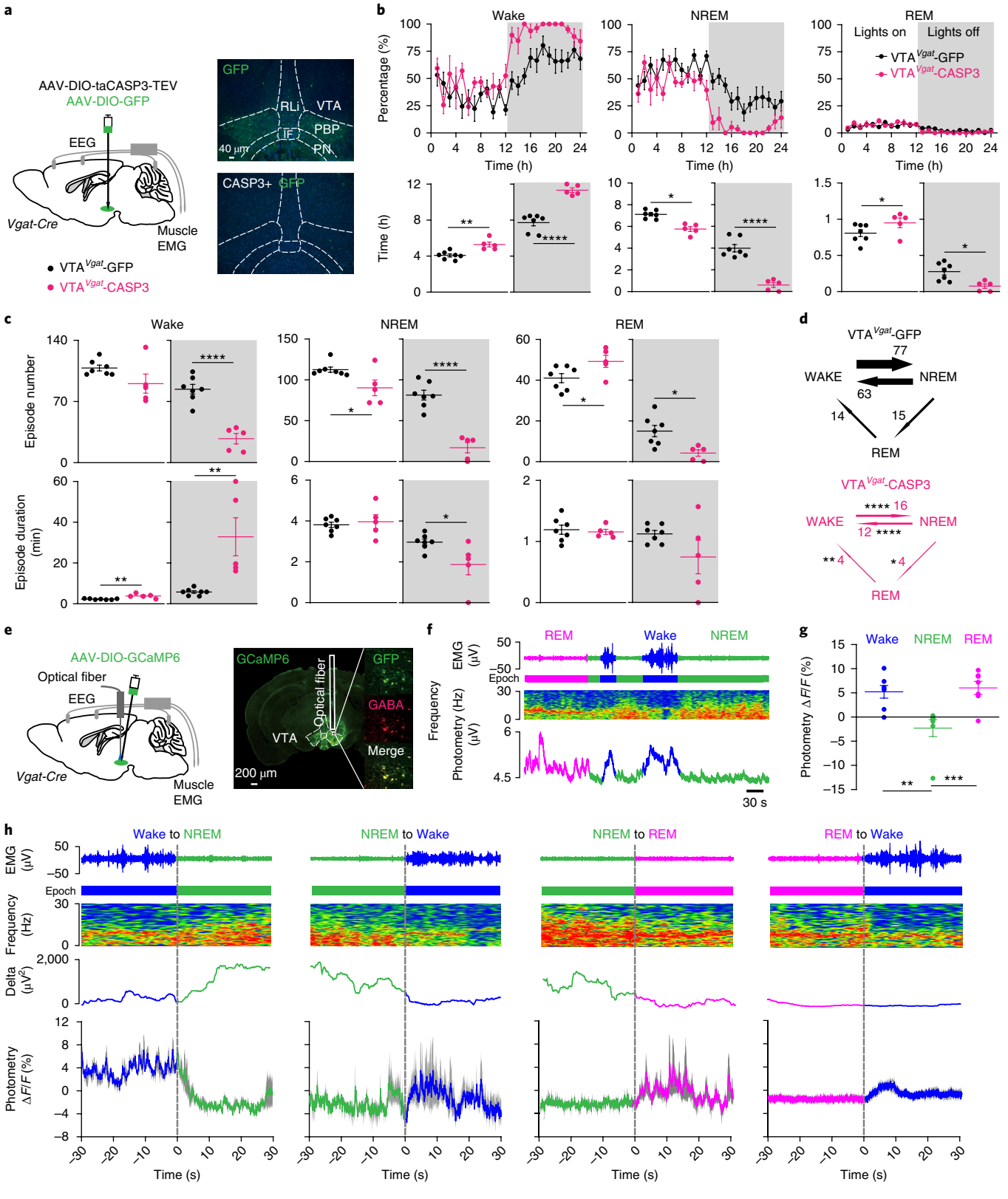

episode duration but without affecting REM sleep duration (Fig. 8c), indicating that the VTA^{Vgat}→LH projection is sufficient to promote and maintain NREM sleep. However, the EEG power did not differ (Supplementary Fig. 14). Because cFos expression was highly elevated in the dentate granule cells (DG) when we inhibited VTA^{Vgat} neurons (Supplementary Fig. 13c), we also opto-stimulated the VTA^{Vgat}→DG projection, but did not observe any effects on sleep or wakefulness (Supplementary Fig. 15a,b). The above results imply that VTA^{Vgat} neurons limit wakefulness by locally inhibiting both VTA glutamatergic and dopaminergic neurons, but also via projection targets (orexin neurons) in the LH.

Discussion

Our search for novel circuits that promote wakefulness identified wake- and REM sleep-active glutamatergic/NOS1 neurons in the VTA (see Supplementary Fig. 16 for schematic summary). By contrast, we found that VTA GABAergic neurons, when artificially activated, produce a profound sedative state, but surprisingly these neurons, such as VTA^{DA} and VTA^{Vglut2} cells, are selectively wake- and REM-active during normal sleep[5]. Because of this mismatch between physiological activity and the outcome of artificial activation, we speculate that VTA^{Vgat} neurons do not physiologically promote natural NREM sleep, but instead restrain wakefulness. This speculation is, in our view, supported by the results of lesioning the VTA^{Vgat} neurons (see below). Alternatively, there could be rare VTA GABAergic neurons, not detected by fiber photometry or in vivo Ca^{2+} imaging, that are NREM sleep-active. Such a cell type might actively induce NREM sleep. At the moment there is no direct evidence for either idea limiting wakefulness or rare NREM-active GABA cells. There are certainly subtypes of GABA neurons in the VTA, for example Pv- and Som-expressing cells, but we found that activating these also induced NREM sleep, although each subtype activated individually does not give the full effect obtained with activating the complete set of VTA^{Vgat} neurons. Future work needs to clarify how the subtypes of VTA^{Vgat} neurons interact to influence sleep and wakefulness.

When VTA^{Vgat} neurons are lesioned this causes permanent sleep loss that persists for months (Supplementary Fig. 11b). It will be interesting to identify metabolic changes produced by this long-term loss of sleep. The effects of the VTA^{Vgat} and VTA^{Vglut2} lesions—that is, more and less wakefulness, respectively—manifest selectively during the 'lights off'/active phase of the mice (Figs. 2b and 6a and Supplementary Fig. 11). This fits with multiunit recordings from mouse VTA neurons, where most cells are under circadian control and fire more during 'lights off'[39].

Loss of VTA^{Vglut2} neurons doubles the number of NREM sleep episodes, and so fragments wakefulness. Nevertheless, the effects of the VTA^{Vgat} lesions on wakefulness (Fig. 6b) are greater than those of lesioning VTA^{Vglut2} cells (Fig. 2b). It is difficult to predict the effects of ablations. For example, histamine neurons, cholinergic neurons, and noradrenergic neurons can be triply lesioned without influencing the baseline amounts of sleep–wake[40], yet the acute activation or inhibition of these cell groups induces large changes in vigilance state[1]. We speculate that VTA^{Vgat} neurons are strategically important as they influence diverse targets, including VTA^{Vglut2}, VTA^{DA}, and LH-orexin neurons. Hence, the loss of VTA^{Vgat} neurons produces large effects. The persistence of this phenotype (chronic wakefulness) post-lesion suggests that no compensation is possible, and perhaps emphasizes the importance of VTA^{Vgat} neurons in regulating vigilance state.

We propose that VTA^{Vgat} neurons limit wakefulness both via projections to arousal-promoting orexin neurons in the LH (Supplementary Fig. 16) and by inhibiting glutamate and dopamine neurons locally in the VTA. As expected[41], we found that some midline VTA^{Vgat} neurons corelease glutamate, although the ratio of optically evoked IPSCs to EPSCs was about 5:1 in favor of inhibition. In the LH, many (60%) of the VTA^{Vgat} targets are orexinergic neurons, but VTA^{Vgat} terminals could also inhibit wake-promoting GABAergic projection neurons[11,15].

When VTA^{Vgat} neurons are chemogenetically excited the duration of the evoked NREM sleep is remarkable, lasting some 6 h, similar to sedation. Thus, VTA^{Vgat} neurons could, in principle, be a target for novel sedatives that promote a sustained NREM-like sleep (Supplementary Fig. 16). It is surprising that this strong sedative effect arising from activating VTA^{Vgat} neurons has not been noticed. Previous work emphasized that activating VTA GABAergic neurons effects motivational states by inhibiting dopamine neurons in the VTA[42], or by inhibiting cholinergic neurons in the NAc[31]. But in none of these experiments was the EEG recorded, so it is unclear how to interpret the behaviors, especially when decreases in a particular behavior were reported, which could, in fact, be caused by sedation.

Inputs or modulators that physiologically excite VTA^{Vgat} neurons will tend to decrease wakefulness. The LHb is one such nucleus that sends many excitatory glutamatergic projections to GABAergic neurons in the VTA[43]. Thus, strong activation of this LHb pathway would be predicted to induce NREM-like sleep. We have found that the anesthetic propofol requires activation of glutamatergic neurons of the LHb to induce sedation; that is, slow wave (delta) power in the EEG and motor immobility[44]. Downstream of the LHb, this

Fig. 7 | VTA^{Vgat} neurons limit wakefulness in part by locally inhibiting dopamine and Vglut2 neurons in the VTA. a, Mapping axonal projections of VTA^{Vgat} neurons. AAV-DIO-ChR2-EYFP was delivered into the VTA of *Vgat-ires-Cre* mice, and axons in the local VTA and projecting to the LH were strongly labeled. The experiment was repeated independently four times. DG, dentate granule cells; LPO, lateral preoptic area; MCLH, magnocellular nucleus, lateral hypothalamus; MTu, medial tuberomammillary nucleus. **b**, cFos-based activity mapping of brain regions after inhibiting VTA^{Vgat} neurons. In VTA^{Vgat}-hM4D$_i$ mice, cFos protein expression is found in neurons of the VTA and LH 2 h after saline or CNO i.p. injection at ZT 0. The red in the histology figure is the primary fluorescence of the hM4D$_i$-mCherry-positive axons; the cFos immunohistochemistry is shown in green. The experiment was repeated independently six times. **c**,**d**, Investigating the local transmitter properties of VTA^{Vgat} neurons in the midline VTA. Acute brain slice electrophysiology was performed on non-Vgat neurons in the midline VTA area in *VTA^{Vgat}-ChR2-EYFP* mice. Non-Vgat cells were visually selected by YFP-negative signals and, after whole-cell status was successfully achieved, a 5-ms single blue light-emitting diode light pulse was given to the local VTA area. The percentages of recorded non-Vgat cells which had oIPSCs only, or oEPSCs only, or both oIPSCs and oEPSCs, were: oIPSC only, 6.25% ($n=1$); oIPSC and oEPSC (oIPSC:oEPSC), 81.25% ($n=13$); oEPSC only, 12.5% ($n=2$). The relative amplitude ratio of the oIPSC peaks versus the oEPSC peaks of non-Vgat cells was 5.71 ± 1.8 ($n=16$). **d**, Heat map for the single-cell PCR of patched cells. The genes tested for were: *Slc17a6* (*vglut2*); *Slc6a3* (*dat*), *Slc32a1* (*vgat*), *th*, and *gad1*. **e**, VTA^{Vgat} neurons inhibit wakefulness in part by inhibiting dopamine neurons. Dopamine receptor D1 and D2/3 antagonists (SCH23390 and raclopride, respectively) were injected into VTA^{Vgat}-hM4D$_i$ mice 30 min before saline or CNO injection. Percentages and times for wake were scored after saline or CNO injection (saline: $n=4$ mice; antagonists: $n=5$ mice; CNO: $n=4$ mice; CNO + antagonists: $n=4$ mice). **f**, Local inhibition from VTA^{Vgat} neurons limits wakefulness. A cannula was placed into the VTA of VTA^{Vgat}-hM3Dq mice, and mice were given gabazine 10 min before saline or CNO i.p. injection. Percentages and times for wake were scored (saline: $n=6$ mice; gabazine: $n=7$ mice; CNO: $n=8$ mice; CNO + gabazine: $n=6$ mice). *P <0.05; for **e** and **f**, repeated measures two-way ANOVA and Bonferroni–Holm post hoc test. All error bars represent s.e.m. For detailed statistical information, see Supplementary Table 1.

mechanism could include the activation of the VTA^{Vgat} neurons, including those GABAergic cells in the rostromedial tegmental nucleus at the posterior end of the VTA[45].

As with VTA^{Vgat} neurons, the extreme wakefulness produced by stimulating VTA$^{Vglut2/Nos1}$ neurons may not have been noticed before because no EEG analysis was performed. We found that the midline VTA$^{Vglut2/Nos1}$ neurons promote wakefulness, in part through the NAc and in part through the LH. The VTA$^{Vglut2/Nos1}$ terminals in the LH could excite GABAergic projection neurons that in turn promote wakefulness[11,15], as well as exciting orexin neurons. On the other hand, because lesioning the NAc increases wakefulness[46,47], this implies that NAc GABAergic projection neurons limit wakefulness, or are actively inducing NREM sleep. If terminals of VTA^{DA} neurons are stimulated in the NAc, wakefulness is produced[5]. This is similar to stimulating the VTA$^{Vglut2/Nos1}$ terminals. However, since the wake-promoting effect of VTA$^{Vglut2/Nos1}$ neurons is not blocked by dopamine receptor antagonists, it could be that the wake-promoting dopamine terminals do so by promoting glutamate release in the NAc. Similar to our findings, the paraventricular thalamus also promotes wakefulness by sending glutamatergic projections to the NAc[17]. It could be that glutamate inputs local GABA neurons in the NAc, which then inhibit the NREM sleep-promoting GABAergic projection neurons. In any case, the NAc is probably a core part of the wake-promoting circuitry.

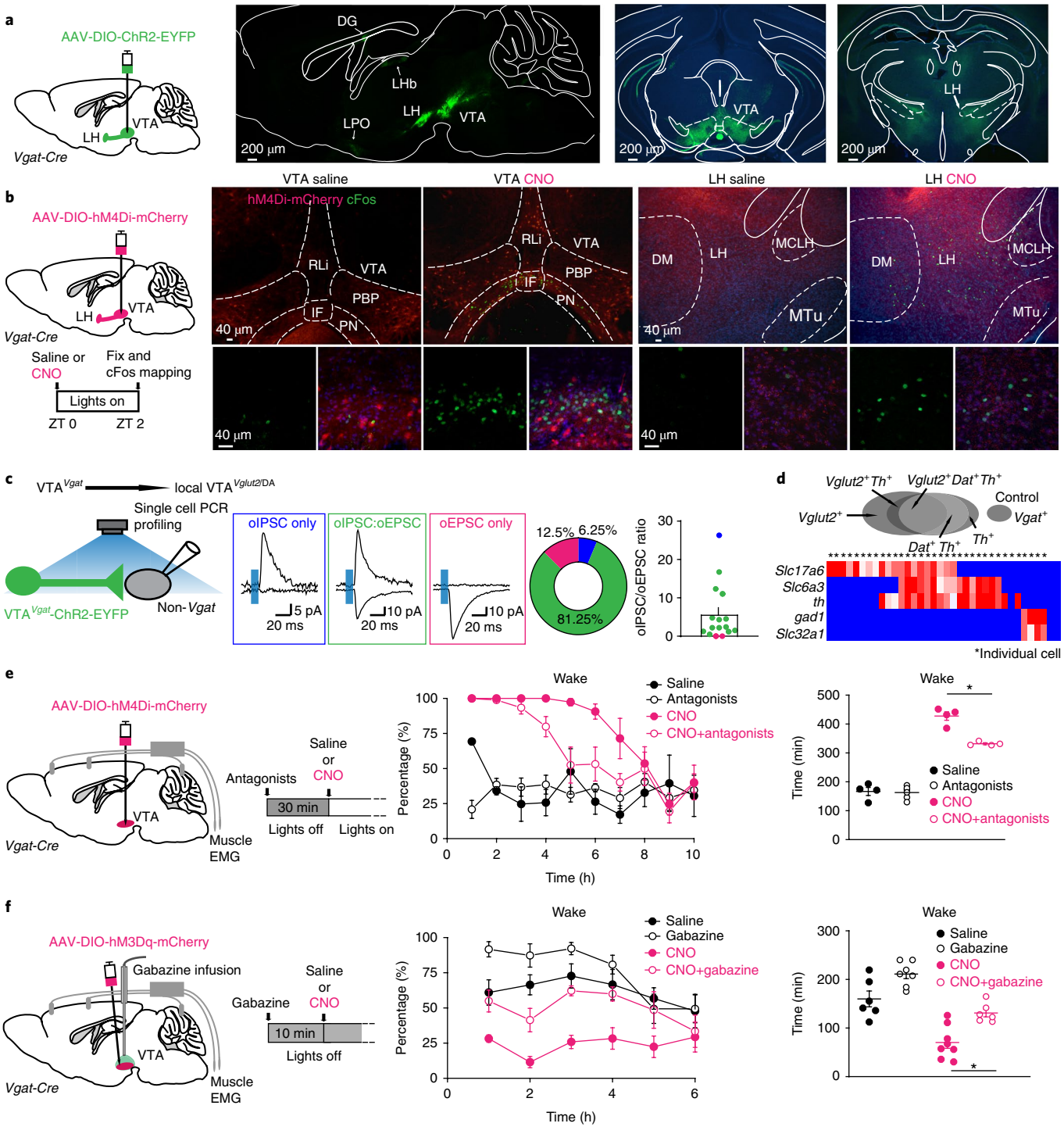

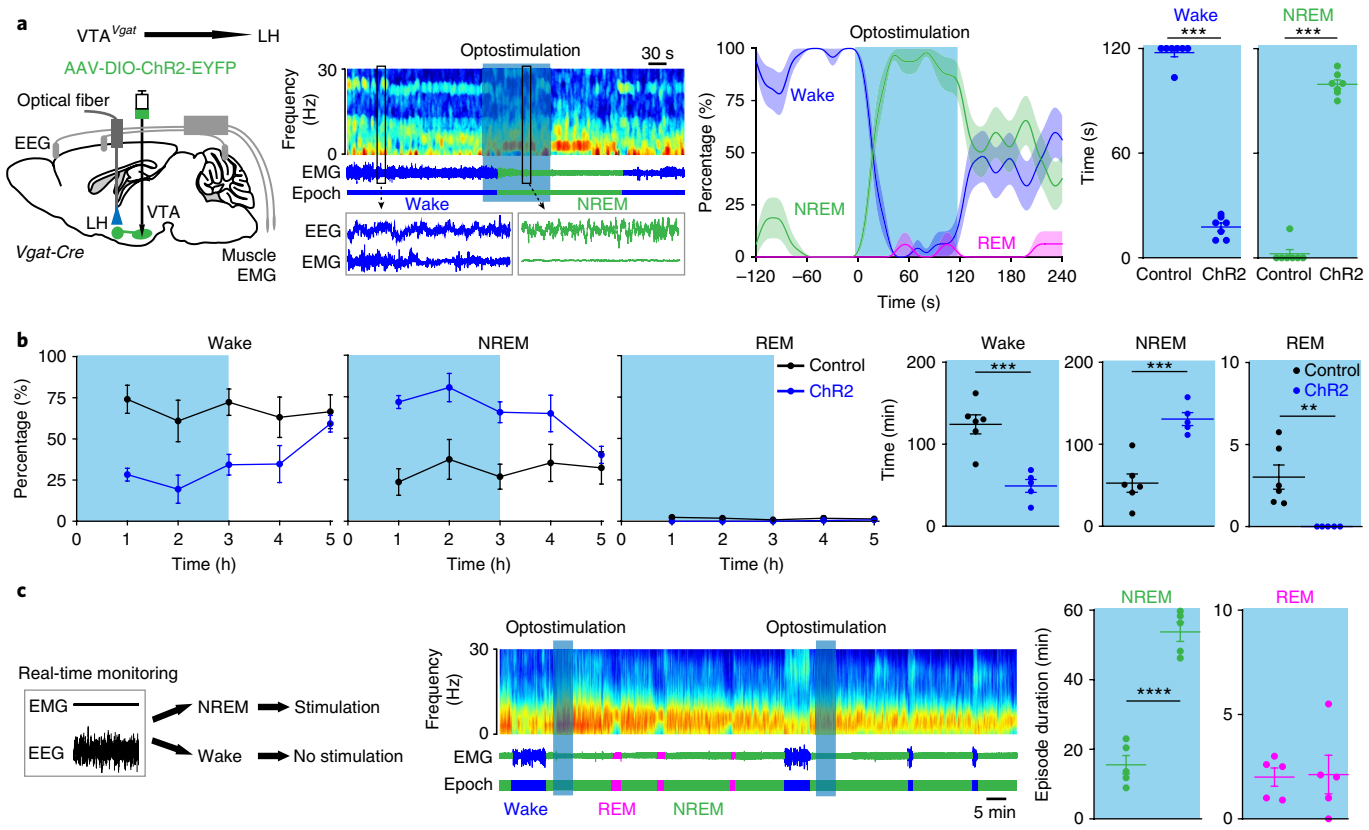

Fig. 8 | VTA^{Vgat} neurons inhibit wakefulness in part via projections to the LH. a,**b**, To functionally test the VTA^{Vgat}→LH projections, an optical fiber was placed into the LH area of VTA^{Vgat}-ChR2-EYFP mice. **a**, Mice were given 120 s of optostimulation (20 Hz) during their active period (during the 'lights off' period) and the percentages and times for wake and NREM sleep were scored (control: $n=7$ mice, 16 trials; ChR2: $n=7$ mice, 16 trials). The envelopes in the graph indicate s.e.m. **b**, VTA^{Vgat}-ChR2-EYFP mice (control: $n=6$ mice; ChR2: $n=5$ mice) were given 3 h of optostimulation during the active period ('lights-off' period) and the percentages and times for wake, NREM, and REM sleep were scored. **c**, Mice were given 5 min of optostimulation when NREM sleep occurred (control: $n=5$ mice, 5 trials; ChR2: $n=5$ mice, 5 trials). The durations of NREM and REM sleep were scored. $^{**}P<0.01$, $^{***}P<0.001$, $^{****}P<0.0001$; for **a**, two-sided Mann–Whitney *U* test; for **b** and **c**, two-sided unpaired *t* test. All error bars represent s.e.m. Shaded regions represent s.e.m. For detailed statistical information, see Supplementary Table 1.

Similar to GABA and glutamate, NOS1 associates with neurons regulating both wakefulness and sleep[21,48]. A recent report found that *Vglut2*/*Nos1* projection neurons in the supramammillary nucleus promote wakefulness when chemogenetically activated[14]. Our CNO injections to activate mammillary *Vglut2* neurons did not increase wakefulness (Fig. 1j). The reason for the difference is unclear, but in principle there could be a continuous population of *Vglut2*/*Nos1* cells from the VTA through to the supramammillary nucleus.

What is the significance of the VTA$^{Vglut2/Nos1}$ or the VTA^{Vgat} neurons being REM-active? Activating the VTA$^{Vglut2/Nos1}$ or the VTA^{Vgat} neurons did not produce REM sleep, and activating VTA^{Vgat} neurons during NREM sleep did not alter REM sleep duration (Fig. 8c). Therefore, the VTA^{Vglut2} and VTA^{Vgat} neurons respond to the primary REM sleep-inducing circuitry, but do not induce or maintain REM sleep.

In summary, our findings on VTA$^{Vglut2/Nos1}$ and VTA^{Vgat} neurons, and other recent discoveries on dopamine VTA neurons[5], identify the VTA as a critical center regulating wakefulness. The VTA is exceptionally well connected, receiving glutamate and GABA inputs from nearly all brain areas[42,43,49,50], making it well suited to serve as an integrator of vigilance state. This should be considered when designing experiments to look at the role of the VTA in reward-directed, goal-directed, and social behaviors.

Online content

Any methods, additional references, Nature Research reporting summaries, source data, statements of data availability and associated accession codes are available at https://doi.org/10.1038/s41593-018-0288-9.

Received: 16 July 2018; Accepted: 9 November 2018;
Published online: 17 December 2018

References

1. Scammell, T. E., Arrigoni, E. & Lipton, J. O. Neural circuitry of wakefulness and sleep. *Neuron* **93**, 747–765 (2017).
2. Weber, F. & Dan, Y. Circuit-based interrogation of sleep control. *Nature* **538**, 51–59 (2016).
3. Saper, C. B. & Fuller, P. M. Wake–sleep circuitry: an overview. *Curr. Opin. Neurobiol.* **44**, 186–192 (2017).
4. Gent, T. C., Bassetti, C. & Adamantidis, A. R. Sleep–wake control and the thalamus. *Curr. Opin. Neurobiol.* **52**, 188–197 (2018).
5. Eban-Rothschild, A., Rothschild, G., Giardino, W. J., Jones, J. R. & de Lecea, L. VTA dopaminergic neurons regulate ethologically relevant sleep–wake behaviors. *Nat. Neurosci.* **19**, 1356–1366 (2016).
6. Yu, X. et al. Wakefulness is governed by GABA and histamine cotransmission. *Neuron* **87**, 164–178 (2015).
7. Cho, J. R. et al. Dorsal raphe dopamine neurons modulate arousal and promote wakefulness by salient stimuli. *Neuron* **94**, 1205–1219.e8 (2017).
8. Oishi, Y. et al. Activation of ventral tegmental area dopamine neurons produces wakefulness through dopamine D_2-like receptors in mice. *Brain Struct. Funct.* **222**, 2907–2915 (2017).
9. Kosse, C., Schöne, C., Bracey, E. & Burdakov, D. Orexin-driven GAD65 network of the lateral hypothalamus sets physical activity in mice. *Proc. Natl Acad. Sci. USA* **114**, 4525–4530 (2017).
10. Schöne, C., Apergis-Schoute, J., Sakurai, T., Adamantidis, A. & Burdakov, D. Coreleased orexin and glutamate evoke nonredundant spike outputs and computations in histamine neurons. *Cell Rep.* **7**, 697–704 (2014).

11. Herrera, C. G. et al. Hypothalamic feedforward inhibition of thalamocortical network controls arousal and consciousness. *Nat. Neurosci.* **19**, 290–298 (2016).
12. Anaclet, C. et al. Basal forebrain control of wakefulness and cortical rhythms. *Nat. Commun.* **6**, 8744 (2015).
13. Xu, M. et al. Basal forebrain circuit for sleep–wake control. *Nat. Neurosci.* **18**, 1641–1647 (2015).
14. Pedersen, N. P. et al. Supramammillary glutamate neurons are a key node of the arousal system. *Nat. Commun.* **8**, 1405 (2017).
15. Venner, A., Anaclet, C., Broadhurst, R. Y., Saper, C. B. & Fuller, P. M. A novel population of wake-promoting GABAergic neurons in the ventral lateral hypothalamus. *Curr. Biol.* **26**, 2137–2143 (2016).
16. Gent, T. C., Bandarabadi, M., Herrera, C. G. & Adamantidis, A. R. Thalamic dual control of sleep and wakefulness. *Nat. Neurosci.* **21**, 974–984 (2018).
17. Ren, S. et al. The paraventricular thalamus is a critical thalamic area for wakefulness. *Science* **362**, 429–434 (2018).
18. Weber, F. et al. Regulation of REM and non-REM sleep by periaqueductal GABAergic neurons. *Nat. Commun.* **9**, 354 (2018).
19. Chung, S. et al. Identification of preoptic sleep neurons using retrograde labelling and gene profiling. *Nature* **545**, 477–481 (2017).
20. Sherin, J. E., Shiromani, P. J., McCarley, R. W. & Saper, C. B. Activation of ventrolateral preoptic neurons during sleep. *Science* **271**, 216–219 (1996).
21. Harding, E. C. et al. A neuronal hub binding sleep initiation and body cooling in response to a warm external stimulus. *Curr. Biol.* **28**, 2263–2273.e4 (2018).
22. Anaclet, C. et al. The GABAergic parafacial zone is a medullary slow wave sleep-promoting center. *Nat. Neurosci.* **17**, 1217–1224 (2014).
23. Uygun, D. S. et al. Bottom-up versus top-down induction of sleep by zolpidem acting on histaminergic and neocortex neurons. *J. Neurosci.* **36**, 11171–11184 (2016).
24. Morales, M. & Margolis, E. B. Ventral tegmental area: cellular heterogeneity, connectivity and behaviour. *Nat. Rev. Neurosci.* **18**, 73–85 (2017).
25. Russo, S. J. & Nestler, E. J. The brain reward circuitry in mood disorders. *Nat. Rev. Neurosci.* **14**, 609–625 (2013).
26. Lüscher, C. The emergence of a circuit model for addiction. *Annu. Rev. Neurosci.* **39**, 257–276 (2016).
27. Gunaydin, L. A. et al. Natural neural projection dynamics underlying social behavior. *Cell* **157**, 1535–1551 (2014).
28. Hung, L. W. et al. Gating of social reward by oxytocin in the ventral tegmental area. *Science* **357**, 1406–1411 (2017).
29. Hnasko, T. S., Hjelmstad, G. O., Fields, H. L. & Edwards, R. H. Ventral tegmental area glutamate neurons: electrophysiological properties and projections. *J. Neurosci.* **32**, 15076–15085 (2012).
30. Taylor, S. R. et al. GABAergic and glutamatergic efferents of the mouse ventral tegmental area. *J. Comp. Neurol.* **522**, 3308–3334 (2014).
31. Creed, M. C., Ntamati, N. R. & Tan, K. R. VTA GABA neurons modulate specific learning behaviors through the control of dopamine and cholinergic systems. *Front. Behav. Neurosci.* **8**, 8 (2014).
32. Tan, K. R. et al. GABA neurons of the VTA drive conditioned place aversion. *Neuron* **73**, 1173–1183 (2012).
33. Taylor, N. E. et al. Optogenetic activation of dopamine neurons in the ventral tegmental area induces reanimation from general anesthesia. *Proc. Natl Acad. Sci. USA* **113**, 12826–12831 (2016).
34. Paul, E. J. et al. nNOS-expressing neurons in the ventral tegmental area and substantia nigra pars compacta. *eNeuro* 5, e0381-18 (2018).
35. Qi, J. et al. VTA glutamatergic inputs to nucleus accumbens drive aversion by acting on GABAergic interneurons. *Nat. Neurosci.* **19**, 725–733 (2016).
36. Yamaguchi, T., Wang, H. L., Li, X., Ng, T. H. & Morales, M. Mesocorticolimbic glutamatergic pathway. *J. Neurosci.* **31**, 8476–8490 (2011).
37. Gomez, J. L. et al. Chemogenetics revealed: DREADD occupancy and activation via converted clozapine. *Science* **357**, 503–507 (2017).
38. van Zessen, R., Phillips, J. L., Budygin, E. A. & Stuber, G. D. Activation of VTA GABA neurons disrupts reward consumption. *Neuron* **73**, 1184–1194 (2012).
39. Fifel, K., Meijer, J. H. & Deboer, T. Circadian and homeostatic modulation of multi-unit activity in midbrain dopaminergic structures. *Sci. Rep.* **8**, 7765 (2018).
40. Blanco-Centurion, C., Gerashchenko, D. & Shiromani, P. J. Effects of saporin-induced lesions of three arousal populations on daily levels of sleep and wake. *J. Neurosci.* **27**, 14041–14048 (2007).
41. Root, D. H. et al. Single rodent mesohabenular axons release glutamate and GABA. *Nat. Neurosci.* **17**, 1543–1551 (2014).
42. Nieh, E. H. et al. Inhibitory input from the lateral hypothalamus to the ventral tegmental area disinhibits dopamine neurons and promotes behavioral activation. *Neuron* **90**, 1286–1298 (2016).
43. Faget, L. et al. Afferent inputs to neurotransmitter-defined cell types in the ventral tegmental area. *Cell Rep.* **15**, 2796–2808 (2016).
44. Gelegen, C. et al. Excitatory pathways from the lateral habenula enable propofol-induced sedation. *Curr. Biol.* **28**, 580–587.e5 (2018).
45. Jhou, T. C., Fields, H. L., Baxter, M. G., Saper, C. B. & Holland, P. C. The rostromedial tegmental nucleus (RMTg), a GABAergic afferent to midbrain dopamine neurons, encodes aversive stimuli and inhibits motor responses. *Neuron* **61**, 786–800 (2009).
46. Qiu, M. H., Vetrivelan, R., Fuller, P. M. & Lu, J. Basal ganglia control of sleep–wake behavior and cortical activation. *Eur. J. Neurosci.* **31**, 499–507 (2010).
47. Qiu, M. H. et al. The role of nucleus accumbens core/shell in sleep–wake regulation and their involvement in modafinil-induced arousal. *PLoS One* 7, e45471 (2012).
48. Morairty, S. R. et al. A role for cortical nNOS/NK1 neurons in coupling homeostatic sleep drive to EEG slow wave activity. *Proc. Natl Acad. Sci. USA* **110**, 20272–20277 (2013).
49. Geisler, S., Derst, C., Veh, R. W. & Zahm, D. S. Glutamatergic afferents of the ventral tegmental area in the rat. *J. Neurosci.* **27**, 5730–5743 (2007).
50. Beier, K. T. et al. Circuit architecture of VTA dopamine neurons revealed by systematic input-output mapping. *Cell* **162**, 622–634 (2015).

Acknowledgements

We thank M. Ungless (Faculty of Medicine, Imperial College London) for comments on the manuscript. Our work was supported by the Wellcome Trust (107839/Z/15/Z, N.P.F. and 107841/Z/15/Z, W.W), the UK Dementia Research Institute (W.W. and N.P.F.), the Funds for International Cooperation and Exchange of the National Natural Science Foundation of China (grant no. 81620108012, H.D. and N.P.F.), the China Scholarship Council (Y.M.), a Rubicon Fellowship (019.161LW.010) from the Netherlands Organization for Scientific Research (W.B.), an Imperial College Schrödinger Scholarship (G.M.), and an Imperial College Junior Research Fellowship (J.J.H.). D.B. and J.J.H. were also supported by The Francis Crick Institute, which receives its core funding from Cancer Research UK (FC001055), the Medical Research Council (FC001055), and the Wellcome Trust (FC001055). The Facility for Imaging by Light Microscopy at Imperial College London is in part supported by funding from the Wellcome Trust (grant no. 104931/Z/14/Z) and BBSRC (grant no. BB/L015129/1).

Author contributions

N.P.F. and W.W. conceived and, with X.Y. and H.D., designed the experiments. X.Y., W.L., Y.M., K.T., J.J.H., E.C.H., W.B., G.M., D.W., L.L., J.G., M.C., Y.L., R.Y., D.B., and Q. Y. performed the experiments and/or data analysis. A.L.V. provided the Neurologgers. N.P.F. and W.W. contributed to the data analysis and with H.D. supervised the project. N.P.F., X.Y., and W.W. wrote the paper.

Competing interests

The authors declare no competing interests.

Additional information

Supplementary information is available for this paper at https://doi.org/10.1038/s41593-018-0288-9.

Reprints and permissions information is available at www.nature.com/reprints.

Correspondence and requests for materials should be addressed to H.D. or N.P.F. or W.W.

Methods

Mice. All experiments were performed in accordance with the UK Home Office Animal Procedures Act (1986); all procedures were approved by the Imperial College Ethical Review Committee and the Ethics Committee for Animal Experimentation of Xijing Hospital, Xi'an, and were conducted according to the Guidelines for Animal Experimentation of Chinese Council institutes. The following strains of mice were used: *Vglut2-ires-Cre: Slc17a6*$^{tm2(cre)Lowl}$*/J*, kindly provided by B.B. Lowell, JAX stock 016963[51] ; *Vgat-ires-Cre: Slc32a1*$^{tm2(cre)Lowl}$*/J*, kindly provided by B.B. Lowell, JAX stock 016962[51]; *Nos1-ires-Cre*$^{tm1(cre)Mgmj}$*/J*, JAX stock 017526[52]; *Som-ires-Cre*: *Sst*$^{tm2.1(cre)Zjh/J}$, JAX stock 013044[53]; and *Pv-Cre* B6;*129P2-Pvalb*$^{tm1(cre)Arbr/J}$, JAX stock 008069[54]. All mice used in the experiments were male and aged 8 weeks at the start of the stereotaxic injections and experiments. Mice were maintained on a 12-h light/12-h dark cycle at constant temperature and humidity with ad libitum food and water.

AAV transgene plasmids. pAAV-hSyn-DIO-hM3Dq-mCherry and pAAV-hSyn-DIO-hM4Di-mCherry were gifts from Bryan L. Roth (Addgene plasmids 44361 and 44362)[55]; pAAV-CBA-DIO-GFP was a gift from Edward Boyden (Addgene plasmid 28304); pAAV-EF1α-DIO-taCASP3-TEV was a gift from Nirao Shah (Addgene plasmid 45580)[56]. pAAV-EF1α-DIO-hChR2(H314R)-EYFP was a gift from Karl Deisseroth (Addgene plasmid 20298). AAV2/9-CAG-DIO-GCaMP6f was a gift from HanBio Co. and packaged by BrainVTA.

To create pAAV-hSyn-DIO-GCaMP6s, we used the GCaMP6s reading frame from pGP-CMV-GCaMP6s-EGFP (a gift from Douglas Kim[57], Addgene plasmid 40753). The plasmid pAAV-hSyn-DIO-hM3D$_q$-mCherry (see above) was digested with AscI and NheI, to remove the hM3D$_q$-mCherry reading frame but keeping both sets of loxP sites to give the pAAV-DIO backbone. The modified GCaMP6s reading frame (in-frame mutated to remove AscI and NheI sites) was amplified by PCR from pAAV-hsyn-GCaMP6s, digested with AscI and NheI, and then ligated into the pAAV-DIO backbone to give pAAV-hSyn-DIO-GCaMP6s.

AAV preparation and stereotaxic injections. To produce AAV (capsid serotype 1/2), the adenovirus helper plasmid *pFΔ6*, capsid-plasmids pH21 (AAV1) and pRVI (AAV2), and the relevant pAAV transgene plasmid (see section 'AAV transgene plasmids') were cotransfected into HEK293 cells and the subsequent AAV particles were collected on heparin columns, as described previously[58,59].

To produce retro-AAV-DIO-rc(Chronos-GFP), we used the rAAV2 packaging plasmid, a gift from Alla Karpova and David Schaffer[60] (Addgene plasmid 81070), and the helper plasmid pFΔ6, together with pAAV-EF1α-DIO-rc(Chronos-GFP), a gift from Edward Boyden[61] (Addgene plasmid 62725). These plasmids were cotransfected into HEK293 cells. To purify the retro-AAV we used the AAVpro Purification Kit (all Serotypes) (Takara Clontech, catalog number 6666).

Surgery. Mice were anesthetized with 2% isoflurane in oxygen by inhalation, received buprenorphine injection, and were placed on a stereotaxic frame (Angle Two, Leica Microsystems). The AAV was injected through a stainless steel 33-gauge/15-mm/PST3 internal cannula (Hamilton) attached to a 10-μl Hamilton syringe, at a rate of 0.1 μl min^{-1}.

The injection co-ordinates and volume were:

(PH/MB)$_L$: medial-lateral ML (±0.85 mm), anterior-posterior AP (−2.7 mm), dorsal-ventral DV (−5.05 mm), 1.5 μl + 1.5 μl;
(PH/MB)$_S$: medial-lateral ML (±0.85 mm), anterior-posterior AP (−2.7 mm), dorsal-ventral DV (−5.05 mm), 1 μl + 1 μl;
LH: medial-lateral ML (±1.00 mm), anterior-posterior AP (−1.56 mm), dorsal-ventral DV (−5.20 mm), 100 nl + 100 nl;
Mammillary: medial-lateral ML (±0.86 mm), anterior-posterior AP (−2.7 mm), dorsal-ventral DV (−5.04 mm), 100 nl + 100 nl;
IPN: medial-lateral ML (−0.02 mm), anterior-psoterior AP (−3.52 mm), dorsal-ventral DV (−4.67 mm), 20 nl + 20 nl;
VTA: medial-lateral ML (±0.35 mm), anterior-posterior AP (−3.3 mm), dorsal-ventral DV (−4.25 mm), 50 nl + 50 nl;
PBP of the VTA: medial-lateral ML (±0.54 mm), anterior-posterior AP (−3.52 mm), dorsal-ventral DV (−4.29 mm), 20 nl + 20 nl.

After injection, the cannula was left at the injection site for 5 min and then slowly pulled out. After injections, mice were implanted with 3 gold-plated miniature screw electrodes (−1.5 mm Bregma, +1.5 mm midline; +1.5 mm Bregma, −1.5 mm midline; −1 mm Lambda, 0 mm midline – reference electrode) with 2 EMG wires (AS634, Cooner Wire). The EMG electrodes were inserted between the neck musculature. The EEG/EMG device was affixed to the skull with Orthodontic Resin Power and Orthodontic Resin Liquid (Tocdental).

For the telemetry EEG and EMG surgery, a TL11M2-F20-EET device (Data Science International) was implanted in the abdominal cavity in mice, four wires of which were subcutaneously led to the mouse's neck by a guiding cannula. Mice were then fixed onto the stereotaxic apparatus in a prone position. A pair of wires was imbedded into the bilateral parietal skulls (AP 0.2 mm, ML 1.5 mm, DV −0.1 mm; AP −1.7 mm, ML −0.2 mm, DV −0.1 mm) by the dental cement to record EEG. The other pair of wires was implanted in the neck muscles to monitor the EMG.

For fiber optogenetic experiments, mice received surgical implantation of a monofiberoptic cannula (200 μm; Doric Lenses), after virus injection, above the VTA (AP −3.3 mm, ML 0.13 mm, DV −3.93 mm), NAc (AP 1.1 mm, ML 0.6 mm, DV −4.2 mm), DG (AP −1.94 mm, ML 1 mm, DV −2 mm), and LH (AP −1.4 mm, ML 1.0 mm, DV −5.16 mm). For fiber photometry experiments, mice received surgical implantation of a monofiberoptic cannula (200 μm, respectively; Doric Lenses), after virus injection, above the VTA (AP −3.3 mm, ML 0.13 mm, DV −3.93 mm) to target VTA^{Vglut2} neurons and (AP −3.3 mm, ML 0.35 mm, DV −4.15 mm) to target VTA^{Vgat} neurons and EEG/EMG implants.

The placements of the fibers from all of the experiments are shown in Supplementary Fig. 17.

For the microendoscopic calcium imaging, *Vgat-ires-Cre* mice, which had already been injected with AAV2/9-CAG-DIO-GCaMP6f into the VTA, were allowed to recover from surgery for 3 weeks. They were then re-anesthetized with isoflurane and had TL11M2-F20-EET telemetry devices fitted (see other protocols in the Methods section). The skull was coated with ultraviolet-curable resin. After 20 s exposure to ultraviolet light, a protective coating was formed on the skull. A small hole (1-mm diameter) was drilled on the skull (AP −3.45 mm, ML 1.25 mm). To avoid bleeding or drying of the meninges and brain tissue, saline (0.9% NaCl) was superfused constantly. The tissue drill with a printed circuit board (PCB) bit (500-μm diameter) was fixed on the stereotaxic frame carefully to remove the brain tissue over the target area. By using a micromanipulator (MP285, Sutter), a GRIN lens (diameter 500 μm, length 7.6 mm) was slowly implanted into the VTA (AP −3.3 mm, ML 0.35 mm, DV −4.15 mm). During the insertion process, the lens stayed still for 10 min for every 1 mm insertion. The lens was then secured by dental cement and the part left outside the skull was covered by tissue glue (Kwik-Sil). One week later, the tissue glue was removed. The camera (nVista, Inscopix) was connected with the lens to check the fluorescence signals, and then the camera base (baseplate) was secured to the skull with dental cement. After surgery, mice were allowed to recover for at least 2 weeks before experiments. The positions of the GRIN lens placements for all mice are shown in Supplementary Fig. 17f.

Behavioral protocols and drug treatments. For chemogenetic experiments, CNO (C0832, Sigma, dissolved in saline, 1 mg kg^{-1}) or saline was injected i.p. and the vigilance states recorded. Mice were split into random groups that received either saline or CNO injection. To test for sleep-promoting effects, we injected saline or CNO during the 'lights off' period when the mice were likely to be most active; to test for wake-promoting effects, we injected saline or CNO at the start of the 'lights on' period when the mice had their maximum sleep drive. For the PH/MB^{Vglut2}-hM3Dq mice, LH^{Vglut2}-hM3Dq mice, M^{Vglut2}-hM3Dq mice, IPN^{Vglut2}-hM3Dq mice, VTA^{Vglut2}-hM3Dq mice, VTA^{Nos1}-hM3Dq mice, and VTA^{Vgat}-hM4Di mice, CNO or saline was injected at the start of the 'lights on' sleep phase. For the VTA^{Nos1}-hM4Di mice, VTA^{Vgat}-hM3Dq mice, VTA^{Pv}-hM3Dq mice, VTA^{Som}-hM3Dq mice, and VTA-PBP$^{Nos1/Vgat}$-hM3Dq mice, CNO or saline was injected i.p. during the 'lights off' active phase. For the optogenetic experiments, VTA^{Vglut2}-ChR2-EYFP mice or VTA^{Vglut2}-GFP were opto-stimulated (20 Hz, 1 min) during the 'lights on' phase; VTA^{Vglut2}-ChR2-EYFP→LH or VTA^{Vglut2}-ChR2-EYFP→NAc mice were opto-stimulated (20 Hz, 2 min or 5 Hz, 1 min) during the 'lights on' sleep phase. For chronic optogenetic stimulation: VTA^{Vglut2}-ChR2-EYFP→LH or VTA^{Vglut2}-ChR2-EYFP→NAc mice or NAc^{Vglut2}-Chronos-GFP→VTA mice were opto-stimulated (20 Hz, 2 s, with 58-s interval) at the start of the 'lights on' sleep phase for 3 h; VTA^{Vgat}-ChR2-EYFP→LH mice were stimulated (20 Hz, 2 min) during the 'lights off' active phase. For chronic optogenetic stimulation: VTA^{Vgat}-ChR2-EYFP→LH mice were opto-stimulated (20 Hz, 2 s, with 58-s interval) at the start of the 'lights on' sleep phase for 3 h. To examine the maintenance of NREM sleep, stimulation was performed during the 'lights on' sleep phase and EEG/EMG tracing was observed in a real-time window. The laser was turned on for 5 min when NREM sleep occurred.

Note: in all of the Ca^{2+} photometry experiments we used GCaMP6s, and for the in vivo microscopy experiments for Ca^{2+} imaging we used GCaMP6f. For the photometry experiments, the Ca^{2+} signal of VTA^{Vglut2}-GCaMP6 or VTA^{Vgat}-GCaMP6 mice was measured for 2–6 h during both the 'lights off' wake phase and the 'lights on' sleep phase. To challenge the mice with novel objects or females, novel objects or female mice were put in the home cage during the 'lights off' wake phase and the Ca^{2+} signal of the VTA^{Vglut2}-GCaMP6 mice was measured.

For the chemogenetic pharmacological experiments, VTA^{Vglut2}-hM3Dq, VTA^{Nos1}-hM3Dq, or VTA^{Vgat}-hM4Di mice were injected (i.p.) with dopamine receptor D1 (SCH23390 0.03 mg kg^{-1}) and D2/3 receptor antagonists (raclopride 2 mg kg^{-1}) and, 30 min after the antagonists' injection, the mice received a saline or CNO (1 mg kg^{-1}) i.p. injection, as previously reported[8]. For VTA^{Vgat}-hM3Dq mice, gabazine (0.001 μg) or saline (300 nl) was infused through a gilded cannula according to a previous study[62]. Then, 10 min after infusion, the mice received saline or CNO (1 mg kg^{-1}) by i.p. injection.

Locomotor activity. The locomotor activity was detected in an activity test chamber (Med Associates) with ANY-maze video tracking system. We injected saline or CNO (1 mg kg^{-1}) i.p. at the start of the 'lights on' period when the mice had their maximum sleep drive, and we performed the locomotion experiment 30 min after injection. The behavior was recorded by a video tracking system

(ANY-maze) using a camera (FUJIFILM) and measured by ANY-maze software (Stoelting).

EEG analysis, fiber photometry, microendoscopic calcium imaging, and sleep–wake behavior. *EEG and EMG.* EEG and EMG signals were recorded using Neurologger 2A devices[63] or TL11M2-F20-EET telemetry devices and dataquest ART (version 4.33). NREM sleep, REM sleep, and wake states were first automatically classified using a sleep analysis software, Spike2 or NeuroScore, and then manually scored.

For the fiber photometry[27], a Grass SD9 stimulator was used to control a 473-nm diode-pumped solid-state blue laser with fiber coupler (Shanghai Laser & Optics Century). The laser light was passed through a single-source fluorescence cube (FMC_GFP_FC, Doric Lenses) through an optical fiber patch cord (Ø 200 µm, 0.22 numerical aperture, Doric Lenses). From the filter cube, a multimodal optical patch cord (Ø 200 µm, 0.37 numerical aperture, Doric Lenses) was connected to the mouse chronically implanted fiber (Ø 200 µm, 0.37 numerical aperture) with a ceramic split mating sleeve ferrule (Thorlabs). The GCaMP6 output was then filtered at 500–550 nm using a second dichroic in the fluorescence cube and converted to voltage by an amplified photodiode (APD-FC, Doric Lenses). The photodiode output was amplified by a lock-in amplifier (SR810, Stanford Research Systems), also used to drive the laser at 125 Hz with an average power of 80 µW at the fiber tip. The signal was then digitized using a CED 1401 Micro Box (Cambridge Electronic Design) and recorded at 1 kHz using Spike2 software (Cambridge Electronic Design).

Photometry. The photometry signal was matched with the EEG and EMG recordings. For each experiment, the photometry signal F was converted to $\Delta F/F$ by $\Delta F/F(t) = (F(t) - \text{median}(F))/\text{median}(F)$[5]. In some recordings, we observed a decay of photometry signal at the beginning of the recording. All of the sessions were selected after the photometry signal became stable. For the sleep–wake analysis, we performed the recordings in 3–4 sessions per mouse, each 1–6-h long, and 1 session for 8 h. To analyze vigilance states for wake, NREM, and REM sleep, we selected all of the sessions in which mice had all three states[5], and we calculated the $\Delta F/F$ photometry ratio during the contiguous three vigilance states. To analyze the transitions for vigilance states, we selected one randomly chosen session per mouse.

For the microendoscopic Ca^{2+} imaging[64], the signal was recorded with the nVista HD system (Inscopix). We analyzed the Ca^{2+} imaging data using ImageJ plug-ins and custom MATLAB script. Video acquisitions were corrected for movement artifacts using TurboReg. Mosaic (Inscopix) was used to analyze the data using principal component analysis-independent component analysis (PCA-ICA) as described in previous studies[65,66]. The $\Delta F/F$ ratio was calculated as $\Delta F/F(t) = (F(t) - \text{median}(F))/\text{median}(F)$. Ca^{2+} traces and $\Delta F/F$ were matched to the EEG/EMG, which was simultaneously recorded with the Ca^{2+} imaging data.

Immunohistochemistry. Mice were transcardially perfused with 4% paraformaldehyde (Thermo Scientific) in PBS (Sigma). Brains were removed and left in 30% sucrose/PBS. Then, 40- or 60-µm-thick coronal sections were cut using a Leica VT1000S vibratome. Free-floating sections were washed in PBS 3 times for 5 min, permeabilized in PBS plus 0.4% Triton X-100 for 30 min, and blocked by incubation in PBS plus 5% normal goat serum (Vector), 0.2% Triton X-100 for 1 h.

Sections were incubated with primary antibody diluted in PBS plus 2% normal goat serum overnight at 4 °C in a shaker. Incubated slices were washed 3 times in PBS for 10 min, incubated for 2 h with secondary antibody (Molecular Probes) in PBS, and subsequently washed 4 times in PBS for 10 min (all at room temperature).

Primary antibodies used: rabbit polyclonal cFos (1:4,000, Santa Cruz), rat monoclonal mCherry (1:2,000, ThermoFisher), rabbit polyclonal GFP (1:1,000, ThermoFisher), mouse monoclonal tyrosine hydroxylase (1:2,000, Sigma), mouse monoclonal NOS1 (1:200, Santa Cruz), mouse monoclonal NOS1 (1:200, Sigma), rat monoclonal somatostatin (1:1,000, Merck), mouse monoclonal parvalbumin (1:1,000, Merck), and mouse monoclonal Orexin-A (1:200, Santa Cruz). Secondary antibodies were Alexa Fluor 488 goat anti-rabbit, Alexa Fluor 488 goat anti-mouse, Alexa Fluor 594 goat anti-rabbit, Alexa Fluor 594 goat anti-mouse, and Alexa Fluor 594 goat anti-rat (1:1,000, Invitrogen).

Slices were mounted on slides, embedded in Mowiol (with 4,6-diamidino-2-phenylindole), cover-slipped, and analyzed using an upright fluorescent microscope (Nikon Eclipse 80i, Nikon), a Zeiss LSM 510 inverted confocal microscope, or a Leica SP5 MP confocal microscope (Facility for Imaging by Light Microscopy, Imperial College London). Images were acquired using Z-scan.

Acute brain slice electrophysiology and single-cell RT–PCR from the midline VTA area of VTAVgat-ChR2-EYFP mice. *Slice preparation.* VTA^{Vgat}-ChR2-EYFP mice were killed by cervical dislocation. Following decapitation, the brains were quickly removed and placed into cold oxygenated N-Methyl-D-glucamine (NMDG) solution (in mM: NMDG 93, HCl 93, KCl 2.5, NaH_2PO_4 1.2, $NaHCO_3$ 30, HEPES 20, glucose 25, sodium ascorbate 5, Thiourea 2, sodium pyruvate 3, $MgSO_4$ 10, $CaCl_2$ 0.5). Coronal brain slices (220-µm thickness) encompassing the midline VTA were obtained using a vibratome (Vibrating Microtome 7000smz-2, Campden Instruments). Slices were kept in NMDG solution at 33°C for 15 min with constant oxygenation, transferred to fully oxygenated standard aCSF (in mM: NaCl 120, KCl 3.5, NaH_2PO_4 1.25, $NaHCO_3$ 25, glucose 10, $MgCl_2$ 1, $CaCl_2$ 2), and maintained in a chamber that was gently and continuously aerated with carbogen gas for at least 90 min at room temperature (20–22 °C) before use for electrophysiology.

Electrophysiological recording from midline VTA neurons innervated by VTAVgat neurons in VTAVgat-ChR2-EYFP mice. Slices were transferred to a submersion recording chamber and were continuously perfused at a rate of 4–5 ml min^{-1} with fully oxygenated aCSF at room temperature. For whole-cell recording, patching pipettes at 4–6 MΩ were pulled from autoclaved borosilicate glass capillaries (1.5 mm OD, 0.86 mm ID; Harvard Apparatus, GC150F-10) and filled with RNase-free intracellular solution containing (in mM): 140 K-gluconate, 5 NaCl, 10 HEPES, 0.1 EGTA, 2 $MgCl_2$, 2 Mg-ATP, and 0.3 Na-GTP (pH 7.35, osmolality 285 mOsm); or 125 KCl, 20 NaCl, 10 HEPES, 1 EGTA, 1 $CaCl_2$, 1 $MgCl_2$, 2 Mg-ATP, and 0.5 Na-GTP (pH 7.35, osmolality 285 mOsm). Neurobiotin (0.1%) was included in the intracellular solutions to identify the cell position and morphology following recording. Recordings were performed in current clamp or voltage clamp mode using a Multiclamp 700B amplifier (Molecular Devices). Access and input resistances were monitored throughout the experiments using a 5-mV voltage step. The access resistance was typically <20 MΩ, and results were discarded if resistance changed by >20%. Membrane capacitance was measured under voltage clamp at −50 mV using a hyperpolarizing 10-mV, 250-ms step. Membrane capacitance was measured from the change in membrane charge taken from the integrated capacity transients (pClamp, Molecular Devices).

Non-YPF^+ neurons (presumed non-VTA^{Vgat} neurons) were visually identified and randomly selected. To maximize RNA recovery, the internal solution in the patch pipette was limited up to 1 µl. A blue light (470 nM) was delivered by TTL-control light-emitting diode to the entire field through the objective. After the stable voltage clamp was achieved, a single 5 ms light pulse was given at the 30 s inter-sweep interval. The light intensity was adjusted according to the magnitude of the response.

At the end of each recording, cytoplasm was aspirated into the patch pipette, and expelled into a PCR tube containing lysate buffer. The single-cell RT–PCR assays were performed using the Single-Cell to CT Kit (Ambion). The content of the neuron was aspirated into the recording pipette and expelled into cell lysis/DNase I solution. Reverse transcription and complementary DNA pre-amplification were performed according to the kit protocol. Quantitative PCR was performed using the TaqMan Gene Expression Assay system (Applied Biosystems). The mouse TaqMan assay probes were designed by, and purchased from, Invitrogen (ThermoFisher): m18srRNA, Mm03928990_g1; mSlc17a6 (*Vglut2*) Mm00499876_m1; mSlc6a3 (*dat*) Mm00438388_m1; mTh Mm00447557_m1; mGad1: Mm04207432_g1; mSlc32a1 (*Vgat*) Mm00494138_m1. The single-cell gene expression matrix was made by Origin.

Quantification and statistics. All statistical tests were run on Origin 2015 (Origin). The individual tests we used are given in the figure legends and the details are supplied in Supplementary Table 1. All data are given as mean ± s.e.m. unless otherwise stated in the figure legends. No statistical methods were used to predetermine sample sizes but our sample sizes are similar to those reported in previous publications[21,44]. The data met the assumptions of the statistical tests used. Before using any given statistical test we formally tested for normality and equal variances. When we found that the data were non-normal, we used non-parametric tests (details in the relevant figure legends and in Supplementary Table 1). All *t*-tests were two-sided.

We excluded mice in which it was subsequently found that the opto-fibers were misplaced or that there was no AAV transgene expression, or when this expression was in the wrong place. Mice were assigned randomly to the experimental and control groups. When possible, experimental treatments were also randomized. When mice were given drugs verses saline, for example, they received the drug or saline in random order. All experimental data analysis was blinded, including cFos counting, the analysis of EEG data, and animal behavior that was scored from videos.

Reporting summary. Further information on research design is available in the Life Sciences Reporting Summary linked to this article.

Data availability

The datasets generated during and/or analyzed during the current study are available from the corresponding authors on reasonable request.

References

51. Vong, L. et al. Leptin action on GABAergic neurons prevents obesity and reduces inhibitory tone to POMC neurons. *Neuron* **71**, 142–154 (2011).
52. Leshan, R. L. et al. Leptin action through hypothalamic nitric oxide synthase-1-expressing neurons controls energy balance. *Nat. Med.* **18**, 820–823 (2012).
53. Taniguchi, H. et al. A resource of Cre driver lines for genetic targeting of GABAergic neurons in cerebral cortex. *Neuron* **71**, 995–1013 (2011).

54. Hippenmeyer, S. et al. A developmental switch in the response of DRG neurons to ETS transcription factor signaling. *PLoS Biol.* **3**, e159 (2005).
55. Krashes, M. J. et al. Rapid, reversible activation of AgRP neurons drives feeding behavior in mice. *J. Clin. Invest.* **121**, 1424–1428 (2011).
56. Yang, C. F. et al. Sexually dimorphic neurons in the ventromedial hypothalamus govern mating in both sexes and aggression in males. *Cell* **153**, 896–909 (2013).
57. Chen, T. W. et al. Ultrasensitive fluorescent proteins for imaging neuronal activity. *Nature* **499**, 295–300 (2013).
58. Klugmann, M. et al. AAV-mediated hippocampal expression of short and long Homer 1 proteins differentially affect cognition and seizure activity in adult rats. *Mol. Cell. Neurosci.* **28**, 347–360 (2005).
59. Murray, A. J. et al. Parvalbumin-positive CA1 interneurons are required for spatial working but not for reference memory. *Nat. Neurosci.* **14**, 297–299 (2011).
60. Tervo, D. G. et al. A designer AAV variant permits efficient retrograde access to projection neurons. *Neuron* **92**, 372–382 (2016).
61. Klapoetke, N. C. et al. Independent optical excitation of distinct neural populations. *Nat. Methods* **11**, 338–346 (2014).
62. Jennings, J. H. et al. Distinct extended amygdala circuits for divergent motivational states. *Nature* **496**, 224–228 (2013).
63. Anisimov, V. N. et al. Reconstruction of vocal interactions in a group of small songbirds. *Nat. Methods* **11**, 1135–1137 (2014).
64. Flusberg, B. A. et al. High-speed, miniaturized fluorescence microscopy in freely moving mice. *Nat. Methods* **5**, 935–938 (2008).
65. Groessl, F. et al. Dorsal tegmental dopamine neurons gate associative learning of fear. *Nat. Neurosci.* **21**, 952–962 (2018).
66. Chen, K. S. et al. A hypothalamic switch for REM and non-REM sleep. *Neuron* **97**, 1168–1176.e4 (2018).

nature research

Corresponding author(s): William Wisden, Hailomng Dong, Nick Franks

Reporting Summary

Nature Research wishes to improve the reproducibility of the work that we publish. This form provides structure for consistency and transparency in reporting. For further information on Nature Research policies, see Authors & Referees and the Editorial Policy Checklist.

Statistical parameters

When statistical analyses are reported, confirm that the following items are present in the relevant location (e.g. figure legend, table legend, main text, or Methods section).

n/a	Confirmed	
☐	☒	The exact sample size (*n*) for each experimental group/condition, given as a discrete number and unit of measurement
☐	☒	An indication of whether measurements were taken from distinct samples or whether the same sample was measured repeatedly
☐	☒	The statistical test(s) used AND whether they are one- or two-sided *Only common tests should be described solely by name; describe more complex techniques in the Methods section.*
☒	☐	A description of all covariates tested
☐	☒	A description of any assumptions or corrections, such as tests of normality and adjustment for multiple comparisons
☐	☒	A full description of the statistics including central tendency (e.g. means) or other basic estimates (e.g. regression coefficient) AND variation (e.g. standard deviation) or associated estimates of uncertainty (e.g. confidence intervals)
☐	☒	For null hypothesis testing, the test statistic (e.g. *F*, *t*, *r*) with confidence intervals, effect sizes, degrees of freedom and *P* value noted *Give P values as exact values whenever suitable.*
☒	☐	For Bayesian analysis, information on the choice of priors and Markov chain Monte Carlo settings
☒	☐	For hierarchical and complex designs, identification of the appropriate level for tests and full reporting of outcomes
☒	☐	Estimates of effect sizes (e.g. Cohen's *d*, Pearson's *r*), indicating how they were calculated
☐	☒	Clearly defined error bars *State explicitly what error bars represent (e.g. SD, SE, CI)*

Our web collection on statistics for biologists may be useful.

Software and code

Policy information about availability of computer code

Data collection	To collect sleep-wake data, we used Downloader (Evolocus) and Spike2 (Cambridge Electronic Design) or Dataquest ART (version 4.33); we used WinWCP (Version 4.1.2) and WinEDR (Version 3.0.9) for electrophysiology experiments (Strathclyde Electrophysiology Software) We used video tracking system (ANY-maze) to collect the behavioral data.
Data analysis	We used Spike2 (Cambridge Electronic Design) to analyze sleep-wake data; we used ANY-maze software to analyze behavioral data; we used WinWCP (Version 4.1.2) to analyze electrophysiology data

For manuscripts utilizing custom algorithms or software that are central to the research but not yet described in published literature, software must be made available to editors/reviewers upon request. We strongly encourage code deposition in a community repository (e.g. GitHub). See the Nature Research guidelines for submitting code & software for further information.

Data

Policy information about availability of data

All manuscripts must include a data availability statement. This statement should provide the following information, where applicable:

- Accession codes, unique identifiers, or web links for publicly available datasets
- A list of figures that have associated raw data
- A description of any restrictions on data availability

The datasets generated during and/or analysed during the current study are available from the corresponding author on reasonable request.

Field-specific reporting

Please select the best fit for your research. If you are not sure, read the appropriate sections before making your selection.

☒ Life sciences ☐ Behavioural & social sciences ☐ Ecological, evolutionary & environmental sciences

For a reference copy of the document with all sections, see nature.com/authors/policies/ReportingSummary-flat.pdf

Life sciences study design

All studies must disclose on these points even when the disclosure is negative.

Sample size	No statistical methods were used to pre-determine sample sizes but our sample sizes are similar to those reported in previous publications21,44. The data met the assumptions of the statistical tests used; before using any given statistical test we formally tested for normality and equal variances.
Data exclusions	We excluded mice where it was subsequently found that the placement of the opto-fibers was misplaced or if there was no AAV expression, or AAV expression was in the wrong place.
Replication	The results were obtained on at least 3 cohorts of mice. Additionally, some of the results were reproduced independently between the three arms of the collaboration, in the Xijing hospital China and Imperial and Crick labs.
Randomization	Mice were assigned randomly assigned to the experimental and control groups. When possible, experimental treatments were also randomized. When mice were given drugs verses saline, for example, they received the drug or saline in random order.
Blinding	All experimental data analysis was blinded, including cFOS counting, the analysis of EEG data and animal behaviour that was scored from videos.

Reporting for specific materials, systems and methods

Materials & experimental systems

n/a	Involved in the study
☒	☐ Unique biological materials
☐	☒ Antibodies
☐	☒ Eukaryotic cell lines
☒	☐ Palaeontology
☐	☒ Animals and other organisms
☒	☐ Human research participants

Methods

n/a	Involved in the study
☒	☐ ChIP-seq
☒	☐ Flow cytometry
☒	☐ MRI-based neuroimaging

Antibodies

Antibodies used	Primary antibodies used: rabbit polyclonal cFOS (1:4000, Santa Cruz Biotechnology, UK, sc-52); rat monoclonal mCherry (1:2000, ThermoFisher, M11217); rabbit polyclonal GFP (1:1000, ThermoFisher, A6455); mouse monoclonal TH (1:2000, Sigma, T2928); mouse monoclonal NOS1 (1:200, Santa Cruz, UK, sc-5302); mouse monoclonal NOS1 (1:200, Sigma, N2280); rat monoclonal somatostatin (1:1000, Merck, MAB354); mouse monoclonal parvalbumin (1:1000, Merck, MAB1572); mouse monoclonal Orexin-A (1:200, Santa Cruz, UK, sc-80263). Secondary antibodies were Alexa Fluor ® 488 goat anti-rabbit IgG, Molecular Probes, A11034; Alexa Fluor ® 594 goat anti-mouse IgG, Molecular Probes, A11005; Alexa Fluor ® 488 goat anti-mouse IgG, Molecular Probes, A11001; Alexa Fluor ® 594 goat anti-rabbit IgG, Molecular Probes, A11037; Alexa Fluor ® 594 goat anti-rat IgG Molecular

Probes, A11007. Secondary antibodies were all diluted in 1:1000.

Validation

All antibodies are validated for species by the manufacturer. The EGFP antibodies and mCherry antibodies only stained mouse brain tissue when AAV expressing EGFP- or mCherry- containing proteins was present. The NOS1 antibodies were validated in NOS1 knockout mice as described by Paul et al (see reference in main manuscript). The c-FOS antibody has been used by many investigators and does seem to reflect neuronal activity in its pattern of staining in mouse; it also stains the nucleus of the cell rather than the cytoplasm, as expected of a transcription factor. The TH antibody has been used by many investigators and gives staining in the classical areas such as VTA, substantia nigra and locus ceruleus. The orexin antibody only stains the lateral hypothalamus in mouse, the unique location of orexin neurons.

Eukaryotic cell lines

Policy information about cell lines

Cell line source(s)	HEK293 cells, Sigma-Aldrich, 85120602/CVCL_0045
Authentication	The cell line was authenticated. But the cell line was used only to package AAV and not to produce biological data
Mycoplasma contamination	The cell line tested negative for mycoplasma contamination
Commonly misidentified lines (See ICLAC register)	No commonly misidentified cell lines were used

Animals and other organisms

Policy information about studies involving animals; ARRIVE guidelines recommended for reporting animal research

Laboratory animals	All mice used in the experiments were male and aged 8 weeks at the start of the experiments/surgeries. These lines are described in the Methods section Mouse: Vglut2-ires-Cre: Slc17a6tm2(cre)Lowl/J, Vong et al., 2011 JAX stock 016963 Mouse: Vgat-ires-Cre: Slc32a1tm2(cre)Lowl/J, Vong et al., 2011 JAX stock 016962 Mouse: Nos1-ires-Cretm1(cre)Mgmj/J, Leshan et al., 2012, JAX stock 017526 Mouse: Som-ires-Cre: Ssttm2.1(cre)Zjh/J, Taniguchi et al., 2011, JAX stock 013044 Mouse: Pv-Cre B6;129P2-Pvalbtm1(cre)Arbr/J, Hippenmeyer et al., 2005, JAX stock 008069
Wild animals	The study did not involve wild animals
Field-collected samples	The samples did not involve samples collected from the field